Copy
RM E54H02

NACA

RESEARCH MEMORANDUM

DRAG DATA FOR 16-INCH-DIAMETER RAM-JET ENGINE WITH

DOUBLE-CONE INLET IN FREE FLIGHT AT

MACH NUMBERS FROM 0.7 TO 1.8

By Merle L. Jones, Leonard Rabb, and Scott H. Simpkinson

Lewis Flight Propulsion Laboratory
Cleveland, Ohio

NATIONAL ADVISORY COMMITTEE
FOR AERONAUTICS
WASHINGTON
October 25, 1954

NATIONAL ADVISORY COMMITTEE FOR AERONAUTICS

RESEARCH MEMORANDUM

DRAG DATA FOR 16-INCH-DIAMETER RAM-JET ENGINE WITH DOUBLE-CONE INLET

IN FREE FLIGHT AT MACH NUMBERS FROM 0.7 TO 1.8

By Merle L. Jones, Leonard Rabb, and Scott H. Simpkinson

SUMMARY

The investigation of air-launched ram-jet engines has been extended
to include a study of models with double-cone inlets having a design free-
stream Mach number of 2.4. One of these models was thoroughly instru-
mented along the cowl and external spike in order to obtain detailed drag
data for this type inlet. The model was launched from an airplane at a
pressure altitude of 35,000 feet, rocket-propelled through the transonic
Mach number range to a free-stream Mach number of 1.87, and then deceler-
ated by drag forces back through the transonic range. Drag data are pre-
sented in the form of cowl pressure drag, additive drag, internal drag,
base drag, and total drag. Mass-flow ratios are presented for both the
rocket-on and rocket-off portions of the flight. Equivalent ram-jet
total-temperature ratios are presented with corresponding thrust-minus-
drag coefficients.

INTRODUCTION

The NACA Lewis laboratory has been conducting a series of free-flight
investigations of the transonic and supersonic performance of 16-inch-
diameter ram-jet engines. These engines were launched at high altitudes
from a carrier airplane and were fin-stabilized to follow a zero-lift
trajectory. The engines contained no guidance equipment, and the per-
formance data were obtained by means of telemetering and radar tracking.

All the ram-jet engines had supersonic annular-nose inlets of the
Ferri type. The first series of engines investigated had 25° half-angle
single-cone inlets with the cowl lip positioned to intercept the oblique
shock at a free-stream Mach number of 1.8. The performance data of these
engines have been reported in references 1 to 8. The second series of
engines were designed for a free-stream Mach number of 2.4. The inlets of
these engines differed from the first series of engines not only in design
Mach number, but also in the spike design. The spike consisted of a double
cone with 22° and 35° half-angle cones. These units, designed for a Mach
number of 2.4, required a rocket-booster unit to accelerate them through

the transonic Mach number range. The performance of this engine type has been reported in references 8 and 9.

Detailed drag data for the single-cone inlet models are reported in references 6 and 7. Similarly detailed drag data for the double-cone-inlet ram-jet engine were obtained from 30 telemetered measurements in place of the 12 described in reference 9. The additional space required was made available by removing the ram-jet fuel system and propelling the model by an internally mounted solid-propellant rocket. The effect of ram-jet combustion on air mass flow was simulated by restricting the air flow at the exit with a convergent section. The model was launched from an F-82 carrier airplane at a pressure altitude of 35,000 feet. It was accelerated by the rocket through the transonic Mach number range to a maximum free-stream Mach number of 1.87 and then was decelerated by aerodynamic drag forces to a subsonic Mach number before the flight ended. The performance data obtained are presented herein.

SYMBOLS

The following symbols are used in this report:

A_c　　capture area at cowl lip, 0.976 sq ft

A_{max}　　maximum cross-sectional area, 1.43 sq ft

a_n　　net acceleration (acceleration in a direction along the longitudinal axis of the model), g's

C_D　　drag coefficient based on maximum cross-sectional area, $D/q_0 A_{max}$

C_d　　drag coefficient based on capture area at cowl lip, $D/q_0 A_c$

C_F　　thrust coefficient, $F/q_0 A_{max}$

D　　drag, lb

d　　maximum diameter, 16.19 in.

F　　thrust, lb

f/a　　fuel-air ratio

M　　Mach number

m　　mass flow, slugs/sec

m_0 mass flow in free-stream tube equal in area to capture area, slugs/sec

P   total pressure, lb/sq ft abs

p   static pressure, lb/sq ft abs

q   dynamic pressure, $0.7\ pM^2$, lb/sq ft

Re   Reynolds number based on model length of 15.04 ft

S   axial distance from cowl lip, in.

T   total temperature, $^{\circ}R$

t   static temperature, $^{\circ}R$

x   axial distance from apex of cone, in.

β ratio of maximum possible air flow at a given free-stream Mach number to that which could flow through a free-stream tube of diameter equal to the cowl-lip diameter

η_c combustion efficiency

μ 1 + fuel-air ratio

τ total-temperature ratio, T_4/T_0

Subscripts:

a   additive

b   base

c   cowl

f   friction

i   internal

s   spike

sonic   local sonic flow conditions

t   total

0   station at free stream

2   station in diffuser 4.06 in. downstream of inlet

4   station at exit

APPARATUS AND PROCEDURE

A photograph of the model mounted on the carrier airplane is shown
in figure 1. The inlet was a double-cone type with no internal contrac-
tion in the diffuser and with cone half-angles of 22° and 35°. The cowl
lip was positioned to intercept the first oblique shock at a free-stream
Mach number of 2.4. In order to simulate the mass-flow effects of com-
bustion, the air flow at the exit was restricted by a convergent section.
A sketch of the 16-inch-diameter model showing dimensions and the cowl
lip detail is shown in figure 2. A photograph of the model prior to
mounting on the carrier airplane is shown in figure 3.

The rocket used to propel the model was a 6-KS-3000, T-40 solid-
propellant unit which is rated at 3000 pounds of thrust at sea level for
6 seconds. It weighed 133 pounds fully loaded and 31 pounds after burn-
out. In order to insure satisfactory ignition, the rocket was maintained
at 90° F while on the carrier airplane by an electrically heated blanket.
Heating the rocket also had the effect of increasing the total impulse.

The model was released from the airplane at a pressure altitude of
35,000 feet and a free-stream Mach number of 0.56. Rocket ignition oc-
curred 4.54 seconds after release and lasted until approximately 11.2
seconds after release. The model reached a maximum free-stream Mach num-
ber of 1.87 approximately 10.6 seconds after release; at this time the
drag forces began to exceed the diminishing thrust of the rocket and the
model began to decelerate. After rocket burn-out, the model continued to
decelerate until a free-stream Mach number of 0.65 was reached at ground
impact 57 seconds after release.

A radar-tracking unit, type SCR-584, with optical tracking facili-
ties was used to determine the position of the model in space. An atmos-
pheric survey was conducted by the carrier airplane in order to determine
the ambient pressure and temperature throughout the flight altitude range.
Velocities of the winds aloft were obtained by releasing a weather balloon
and tracking it by radar. These wind velocities were applied to the com-
puted space velocities of the model in order to get the velocity of the
model relative to the air.

The model weighed 449 pounds at release and 347 pounds after rocket
burn-out. Twenty-one pounds of ballast were carried in the nose in order
to obtain a desired center of gravity location of 100.2 inches from the
apex of the cone.

3323

INSTRUMENTATION

The model contained a 10-channel telemetering transmitter with a switching unit which allowed 30 different measurements to be transmitted within a time interval of 0.17 second. A photograph of the telemetering equipment is shown in figure 4. Figure 5 is a close-up view of the switching-unit assembly.

Of the 30 measurements made, 28 were pressure measurements and two were axial accelerations. The cowl surface was instrumented with eight static-pressure taps (see fig. 6). The instrumentation along the center-body is illustrated in figure 7. Eleven static-pressure taps were located along the spike as shown. (The first pressure tap following the micarta insulating block is not visible in the photograph.) In addition, the inlet was instrumented with a flush static-pressure tap and a static-pressure probe. A slotted averaging-type total-pressure probe and a flush static-pressure tap, which were used to measure the air flow in the diffuser, are also shown. Additional pressure measurements were made at the model exit; these included the exit static and total pressures and the base static pressure. The pitot-static tube used to measure the free-stream static and total pressures also served the telemetering unit as an antenna. Two accelerometers measured the axial accelerations - ranges of 0 to -4.5 g's and -6 to +13 g's were used.

METHODS OF CALCULATION

The free-stream Mach number was calculated from the ratio of the free-stream static pressure to the total pressure which was measured at the pitot-static tube. For supersonic Mach numbers, normal-shock corrections were applied to the measured total pressure. The free-stream static pressure was determined from the altitude of the model as obtained from the radar-tracking unit. This information was available only for the first 31 seconds of flight, at which time the model reached an altitude of 18,500 feet. The measured free-stream static pressure was used for the remainder of the flight.

The air flow through the engine was calculated from the measured total pressure and static pressure in the diffuser and the calculated free-stream total temperature. The mass-flow ratio m/m_0 is defined as the ratio of air flowing through the engine to the air which could flow through a free-stream tube of diameter equal to that of the cowl lip. In terms of areas, m/m_0 equals the free-stream tube area divided by the projected lip area.

The internal drag was calculated from the change in total momentum of the internal air flow between the free stream and the engine exit.

The total drag, which was obtained from the model weight and accelerometer data, and the base pressure drag were calculated in accordance with reference 6. The additive, cowl pressure, and spike pressure drags were calculated in accordance with reference 7.

In order to calculate the propulsive thrust coefficient of an equivalent burning ram-jet engine with a straight-pipe exit, it was necessary to determine the total-temperature ratios τ which would be required to produce the observed mass-flow ratios. The calculations for τ were made with the following assumptions: The total-pressure drop across the flame holder was equal to twice the dynamic pressure immediately upstream of the flame holder; the ratio of the total pressure upstream of the flame holder to the free-stream total pressure was equal to the average of the total-pressure ratios near the diffuser inlet and the engine outlet; the gas constant did not change across the combustion chamber; and μ was equal to 1.055. After the flow conditions immediately downstream of the flame holder were determined, the equivalent total temperatures at the exit were calculated from the equations for momentum change and pressure drop due to heat addition in a constant-area duct by an iteration process in which values for the exit Mach number and the specific heat ratio γ were assumed. In addition, calculations were made for the total-temperature ratios and propulsive thrust coefficients which would be produced by a fuel-air ratio of 0.067 and a combustion efficiency of 90 percent. The free-stream conditions used were the same as those observed during the rocket-off portion of the flight. The assumed total-pressure recoveries in the diffuser and the assumed total-pressure drop across the flame holder were the same as those mentioned previously.

The thrust minus drag corresponding to the simulated heat addition was obtained by subtracting the external drag (cowl drag plus additive drag plus estimated friction drag) from the calculated thrust due to the simulated heat addition. The thrust was calculated as the difference between the total momentum of the engine exhaust gases and that of the engine air flow in the free-stream tube.

Only portions of the data were usable during the rocket-on portion of the flight. After the model reached a free-stream Mach number M_0 of 1.15, an unstable condition developed which caused large fluctuations in the accelerations, the spike pressures, and the air flow. The cowl pressures were not affected until near the end of the rocket-on portion of the flight. The unstable condition can be attributed to either rocket chugging or to inlet buzzing resulting from the very low mass-flow ratios. Since no difficulties were experienced with the rocket in prior or subsequent flights, it is more probable that inlet buzzing was responsible for this instability.

RESULTS AND DISCUSSIONS

A plot of the model flight acceleration, altitude, and free-stream Mach number against time is shown in figure 8. The acceleration data during the rocket-on portion of the flight have not been presented because of the unstable operation. The accelerometer indicated high frequency and large amplitude oscillations. It was possible to determine, however, that the maximum acceleration of the model was approximately 10.5 g's. A maximum deceleration of 3.24 g's occurred during rocket tail-off (that portion of the rocket operation when the thrust goes to zero) after which the deceleration decreased to a value of 1.35 g's and remained at that point for the rest of the flight. The free-stream Mach number increased rapidly after rocket ignition to a maximum of 1.87 shortly before rocket burn-out and then decreased gradually to a value of 0.65 at ground impact.

The free-stream static pressure, static temperature, and Reynolds number encountered during flight are presented in figure 9. The Reynolds number is based on a body length of 15.04 feet. Figure 10 shows the variation of mass-flow ratio m/m_0 with free-stream Mach number.

Also shown is the theoretical maximum mass-flow ratio of the inlet for the range of free-stream Mach number encountered during the flight. The exit restriction had the effect of reducing the air flow through the engine and thereby reducing the mass-flow ratio below the critical value. The rocket gases being expelled through the engine outlet during rocket operation provided an additional restriction which further reduced the mass-flow ratio below the critical value. The minimum m/m_0 was 0.260 at a M_0 of 1.10 during the rocket-on portion of the flight, while the corresponding m/m_0 for the rocket-off portion of the flight was 0.475.

Comparison between the theoretical curve and the high mass-flow ratio curve indicates that approximately 10 percent of the maximum mass-flow was being spilled at the inlet during the rocket-off flight. The leveling off of the high mass-flow ratio curve at M_0 above 1.5 is probably an effect of the rocket tail-off. As previously mentioned, the model experienced an unstable operating condition during the rocket-on flight which affected the mass-flow ratios at $M_0 > 1.2$. Therefore, the data which have been presented at Mach numbers greater than 1.2 represent average rather than instantaneous values. At Mach numbers above 1.66, the data have not been presented because of extreme fluctuations in the air flow.

Pressure Recovery

The total-pressure recovery in the diffuser at a station 4.06 inches downstream of the inlet is shown as a function of free-stream Mach

number in figure 11. Data are shown for the rocket-off portion of the flight and part of the rocket-on portion of the flight. Also shown are unpublished data from tests made in the Lewis 8- by 6-foot supersonic wind tunnel on an inlet identical to that reported herein. The mass-flow ratios for the tunnel data are the same as those observed during the rocket-off flight. Although the rocket-off flight data indicate total-pressure recoveries slightly greater than 1.0, the tunnel data indicate recoveries for this inlet very close to 1.0. Agreement between the two are within 2 percent. The rocket-on data indicate high separation losses which are associated with low mass-flow ratios.

<div style="text-align:right">3323</div>

Drag

The total drag of this model with simulated ram-jet combustion consists of cowl pressure drag, additive drag, external friction drag, internal drag, and base pressure drag. Insofar as the performance of a burning ram-jet engine with exit area equal to the maximum cross-sectional area is concerned, only the first three drag components are of interest - the internal drag and base drag would not exist. However, the internal and base drag components are required for correlation of the component drags with the total drag as determined by accelerometer data. These internal drag and base drag data are also of interest in connection with other configurations.

Cowl drag. - Figure 12 presents the effects of mass-flow ratio on the cowl-surface pressure distribution for constant values of free-stream Mach number. The data are presented as a ratio of the measured cowl static pressure to the ambient static pressure p_c/p_0 plotted against the axial distance parameter S/d for a range of free-stream Mach number from 0.70 to 1.80. The higher turning angles around the cowl lip associated with lower mass-flow ratios result in higher velocities with lower pressures. Because of this strong effect of mass-flow ratio on the flow around the cowl lip, the effects of mass-flow ratio on the static-pressure distribution were greatest in the region near the lip ($S/d < 0.1$). The pressure gradient in this region changed from positive to negative in the Mach number range from 0.7 to 1.2. Generally speaking, the effects of mass-flow ratio diminished with increasing values of S/d. The curves indicate that the static pressure along most of the cowl was less than the ambient static pressure. As a result, along these portions of the cowl the force was in the thrust direction. The theoretical curves of $(p_c/p_0)_{sonic}$ are used to denote the static-pressure ratios that would exist along the cowl in local sonic flow. Above a free-stream Mach number of 0.9, the flow over most of the cowl was supersonic - a very small region near the inlet remained subsonic through a M_0 of 1.4 at the higher mass-flow ratios. The sharp break in the curves at $S/d \simeq 0.1$ is a result of the expanding flow around the sharp angle near the cowl lip (see fig. 6). No data are

3323

CQ-2

presented for the low mass-flow ratio (rocket-on operation) at a M_0 of 1.80, because at this point the cowl pressures were affected by the unstable operation.

In the free-stream Mach number range from 0.7 to 1.2 during the rocket-off portion of the flight, the mass-flow ratio remained relatively constant (0.47 to 0.49). For that part of the flight, the data of figure 12 are presented in figure 13 in order to show the effect of M_0 on the cowl-surface pressure distribution at a constant mass-flow ratio.

Figure 13 is a plot of the cowl static-pressure ratio p_c/p_0 against the axial distance parameter S/d for a range of free-stream Mach number from 0.70 to 1.20 at a constant mass-flow ratio. Superimposed upon the figure is the sonic line which locates the local sonic Mach number along the cowl. In the free-stream Mach number range from 0.7 to 0.9, two sonic points existed along the cowl for each M_0. The first sonic point moved upstream from an S/d of 0.05 to an S/d of 0.02 as the M_0 increased from 0.7 to 0.9. The second sonic point moved downstream from an S/d of 0.10 to an S/d of 0.72 as the M_0 increased from 0.7 to 0.9. In the free-stream Mach number range from 1.0 to 1.2, one sonic point existed on the cowl for each M_0. The location of this point remained fairly constant at an $S/d \simeq 0.02$.

The cowl pressure drag coefficient based on the maximum cross-sectional area $C_{D,c}$ is presented in figure 14 as a function of the free-stream Mach number. The negative cowl drag coefficient, which is, in effect, a thrust coefficient, reached a maximum value of 0.19 at a M_0 of 1.05 and a m/m_0 of 0.260 during the rocket-on portion of the flight.

The cowl pressure drag coefficient based on the capture area of the cowl lip $C_{d,c}$ is presented in figure 15 as a function of mass-flow ratio for various free-stream Mach numbers. Because of the limited data, the curves of figure 15 are drawn as straight lines. It is felt that the error involved in this assumption is insignificant for purposes of interpolation, but that linear extrapolation should be avoided. At the lower mass-flow ratios (approximately 0.3), $C_{d,c}$ changes very little as M_0 increases from 0.7 to 1.2. The slopes are approximately constant in the subsonic Mach number range (0.7 to 0.9) and then increase rapidly through the transonic Mach number range (0.9 to 1.2). In the supersonic Mach number range, the slopes decrease again.

Additive drag. - The thrust of a turbojet or ram-jet engine is usually considered as the difference between the total momentum of the gases leaving the engine and the free-stream total momentum of the engine air

flow. This is a purely arbitrary definition of thrust and results in a
term called "additive drag." The additive drag may be defined as the
drag force acting in the axial direction on the entering streamlines to
the engine. This term completes the force envelope on the engine and
makes possible an accurate analysis of the net propulsive force. The
additive drag coefficient based on the maximum cross-section area $C_{D,a}$
is presented against free-stream Mach number in figure 16. Data are pre-
sented from a M_0 of 0.70 to 1.81 when the rocket is not operating. Dur-
ing rocket operation, the data are not presented beyond a M_0 equal to
1.15 because of the unstable operation. It is apparent that the additive
drag was considerably greater during rocket operation (low mass-flow ra-
tios) than during the decelerating portion of the flight. As M_0 in-
creased from 0.70 to 1.15, $C_{D,a}$ increased from 0.045 to 0.218 for the
rocket-off flight and from 0.198 to 0.453 for the rocket-on flight. The
effects of mass flow on the additive drag coefficient can be more easily
observed in figure 17 where additive drag coefficient based on the cowl-
lip projected area $C_{d,a}$ is plotted against mass-flow ratio m/m_0 for
constant free-stream Mach numbers. The additive drag coefficient was ob-
served to increase as the Mach number increased at constant mass-flow ra-
tio. For example, as M_0 increased from 0.80 to 1.10 at m/m_0 of 0.50,
$C_{d,a}$ increased from 0.081 to 0.261. This trend is typical of subsonic
engine operation. Unpublished data from tests made in the Lewis 8- by
6-foot supersonic wind tunnel on an inlet identical to that reported here-
in are also shown in figure 17. The agreement between the tunnel data and
the flight data is very good.

The additive drag of a conical inlet that is operating subcritically
at off-design supersonic free-stream Mach numbers is affected by the rela-
tive mass-flow capacity of the inlet as well as by the cone angle, free-
stream Mach number, and mass-flow ratio (ref. 10). In other words, β is
also an important parameter when additive drag is discussed. The varia-
tion of β with M_0 for the double-cone inlet of this report has been
presented in figure 10. The theoretical effect on the additive drag coef-
ficient of changing β from 1.0 to 0.75 for a 25° half-angle single-cone
diffuser is presented in figure 17 at $M_0 = 1.80$ (ref. 10). Reducing β
from 1.0 to 0.75 at $m/m_0 = 0.612$ theoretically reduced $C_{d,a}$ by 40 per-
cent. For the double-cone inlet of this report, $C_{d,a}$ was 0.470 for
$m/m_0 = 0.612$ and $M_0 = 1.8$ ($\beta = 0.75$). This value is 20 percent greater
than that for the 25° cone inlet operating at a β of 0.75.

The additive drag coefficient calculations as described in refer-
ence 7 included an evaluation of the pressure drag along the spike. The
static-pressure distribution along the spike is presented in figure 18 in

the form p_s/p_0 against the axial distance from the apex of the cone. The data are presented at constant free-stream Mach numbers for the observed mass-flow ratios. At M_0 greater than 1.10, the data are presented for only one mass-flow ratio because of the previously discussed effects of the unstable operation. There is a pronounced effect on the pressure distribution along the spike for a given free-stream Mach number as the mass-flow ratio changes. For example, at $M_0 = 0.90$ and $m/m_0 = 0.474$, the pressure ratio p_s/p_0 rises slightly along the first cone from 1.29 to 1.35 and then drops rapidly along the second cone to a minimum value of 1.0 at $x = 10.56$. For the reduced mass-flow ratio of 0.283, the variation of p_s/p_0 along the spike was very different. The abrupt change in the pressure distribution which occurred at $x = 7.44$ for $m/m_0 = 0.474$ was not observed at $m/m_0 = 0.283$ and the pressure ratio continued to increase gradually all along the spike.

The positive pressure gradient along the initial cone changed only slightly through a M_0 of 1.2 and then became progressively greater at the higher Mach numbers. The theoretical pressure ratio for the initial cone is also indicated in figure 18(g) to (i) for $M_0 = 1.40$ to 1.80.

In computing the spike drag, the spike pressures were integrated from $x = 0$ to $x = 10.56$. The sudden increase in p_s/p_0 beyond $x = 10.56$ was due to the increase in flow area in the diffuser beyond the inlet station.

The effect of free-stream Mach number on the spike pressure distribution for an approximately constant mass-flow ratio (m/m_0 of 0.47 to 0.49) is shown in figure 19 for $M_0 = 0.70$ to 1.20. The curves exhibit a similarity in trend throughout this Mach number range since the flow over the spike was subsonic (the oblique shock attachment to the first cone did not occur until a free-stream Mach number of 1.25 was reached). Except for a very small part of the spike near the inlet at Mach numbers of 0.7 and 0.8, the static pressure along the spike was greater than the free-stream static pressure in the Mach number range from 0.7 to 1.2. The static pressure along the spike increased with increasing Mach number. The spike pressure drag coefficient based on the maximum cross-sectional area $C_{D,s}$ is plotted in figure 20 against the free-stream Mach number.

Additive plus cowl drag. - The additive and cowl drag coefficients are presented in figure 21 in the form of $(C_{D,a} + C_{D,c})$ against free-stream Mach number for the observed mass-flow ratios. Lines of constant mass-flow ratio have been faired through the data points. For m/m_0

equal to 0.47, $(C_{D,a} + C_{D,c})$ increased from 0.082 at a M_0 of 1.00 to 0.208 at a M_0 of 1.20. The maximum observed value of $(C_{D,a} + C_{D,c})$ was 0.327 for $m/m_0 = 0.612$ at a M_0 of 1.81. Also shown in figure 21 are free-flight data for the same type inlet under actual burning conditions (ref. 9) at mass-flow ratios of 0.66 to 0.89 and Mach numbers of 1.55 to 2.00.

Internal drag. - Figure 22 shows the internal drag coefficient $C_{D,i}$ plotted against free-stream Mach number. Because of the unstable operating conditions and resulting unstable air flow, no data are presented for the rocket-on portion of the flight. The internal drag coefficient decreased from 0.119 at a free-stream Mach number of 0.70 to 0.048 at a Mach number of 1.50. The change in the slope of the curve at $M_0 > 1.5$ is probably an effect of the previously mentioned rocket tail-off.

Base-drag. - The base static-pressure ratio p_b/p_0, the base drag coefficient $C_{D,b}$, and the jet static-pressure ratio p_4/p_0 are shown plotted against M_0 in figure 23. The measured values of the exit static pressure p_4 gave unrealistic values of exit Mach number and were considered unreliable. Instead, calculated values of p_4 based on the air flow are shown. An abrupt drop in the base pressure ratio from 0.86 to 0.48, with a resulting rise in drag coefficient from 0.170 to 0.415, occurred in the transonic Mach number range for the rocket-off portion of the flight, but the characteristic transonic break in the data is not present for the rocket-on phase. The abrupt drop in the base pressure was accompanied by a rise in the exit static pressure. The exit pressure continued to rise rapidly because of the choked condition at the exit, while the base pressure tended to level off at a M_0 of 1.07. Also shown are base pressure data from reference 6. Although the data being reported herein exhibit uncharacteristic changes in slopes at M_0 of 0.85 and 0.95 for the rocket-off flight, the data are considered to be valid because of corresponding changes in the total-drag data which are based on data from an independent measurement with the accelerometer.

Total drag. - The total-drag coefficient based on the maximum cross-sectional area $C_{D,t}$ is shown as a function of the free-stream Mach number for the rocket-off portion of the flight in figure 24. These data represent the net force acting on the model as determined from the acceleration data. The drag coefficient dropped from a value of 0.528 at a M_0 of 0.80 to a value of 0.445 at a M_0 of 0.86 and then rose sharply through the transonic range to a maximum value of 0.788 at a M_0 of 1.09.

The values for the total-drag coefficient above a M_0 of 1.5 were indeterminate because of the effect of rocket tail-off.

Figure 25 illustrates the magnitude of the individual drag forces relative to each other and to the total drag for rocket-off conditions. An estimated friction drag based on data presented in reference 7 is used in the figure. The total-drag coefficient is presented as a summation of the component drag coefficients including the estimated friction drag and as a force coefficient which was independently determined from the accelerometer data. Agreement between the two methods is satisfactory. The sum of the cowl, additive, and friction drag coefficients, which would be the external drag coefficient of a burning ram-jet engine with no base area, increased from a minimum value of 0.140 at a M_0 of 0.70 to a maximum value of 0.470 at a M_0 of 1.81. At the low Mach numbers, the friction drag, when compared with the sum of the cowl and additive drags, constituted a large part of the external drag. At the high Mach numbers, the friction drag became a smaller part of the external drag than the cowl plus additive drag. In the transonic Mach number range, the base drag constituted a large part of the total drag and had a very pronounced effect on the shape of the total-drag curve. At a free-stream Mach number of 1.07, the base drag amounted to 53 percent of the total drag, while the external drag amounted to 39 percent of the total drag. At a M_0 of 1.80 the external drag amounted to 75 percent of the total, while the base drag amounted to 21 percent of the total.

Figure 26 illustrates the magnitude of the individual drag forces relative to each other for the first part of the rocket-on flight up to a free-stream Mach number of 1.15. The external drag coefficient increased from 0.255 at a M_0 of 0.70 to 0.460 at a M_0 of 1.15.

Equivalent Heat Addition

Calculations were made to determine the total-temperature ratios τ and the resulting propulsive thrust coefficients $(C_F - C_D)$ for a burning ram-jet engine that was simulated by the restriction to the air flow at the outlet during the rocket-off portion of the flight. These calculations were made for a constant-area combustion chamber. In addition, to indicate the attainable performance of this engine with gasoline fuel, calculations were made to determine mass-flow ratios, propulsive thrust coefficients, and total-temperature ratios where the product of the fuel-air ratio and the combustion efficiency was assumed to be 0.06. The results of these calculations are plotted against M_0 in figure 27. The propulsive thrust coefficient corresponding to the observed mass-flow ratios increases from 0 at M_0 of 0.73, τ of 3.00, and m/m_0 of 0.490

to 0.540 at M_0 of 1.80, τ of 5.18, and m/m_0 of 0.612. The propulsive thrust coefficient corresponding to the assumed $(f/a)(\eta_c) = 0.06$ increases from 0.140 at M_0 of 0.70, τ of 7.06, and m/m_0 of 0.319 to 0.555 at M_0 of 1.80, τ of 5.82, and m/m_0 of 0.567. Also shown in the figure is a curve of the propulsive thrust coefficient of the single-cone inlet engine (model D) reported in reference 8 for the same total-temperature ratios as those calculated for the observed mass-flow ratios. Comparison of the two curves shows the appreciable effect of design Mach number and inlet type on off-design performance. Both these inlets are designed for approximately the same critical τ, $(\tau \approx 3.0)$, but the mass-flow ratio is much lower at a given M_0 and τ for the double-cone inlet than for the single-cone inlet. The effect of the lower mass-flow ratio is a higher additive drag which, in turn, results in a lower propulsive thrust coefficient. For example, at M_0 of 0.80 and τ of 3.11, the propulsive thrust coefficient of the double-cone inlet engine is 76 percent lower than that of the single-cone inlet engine; at M_0 of 1.10 and τ of 3.98, the decrease is 69 percent; and at M_0 of 1.70 and τ of 4.55, the decrease is 21 percent.

SUMMARY OF RESULTS

As part of a series of investigations of the transonic and supersonic performance of 16-inch-diameter ram-jet engines, one model which had a double-cone inlet with a design free-stream Mach number of 2.4 was thoroughly instrumented along the spike and external cowl in order to obtain detailed drag data. The model was rocket-propelled to a maximum free-stream Mach number of 1.87 and then decelerated by drag forces to a Mach number of 0.65 at ground impact. Data obtained from the flight provided the following results:

1. The cowl drag was negative throughout most of the flight, indicating a net thrust force acting on the cowl surface. The negative cowl drag coefficient based on the maximum cross-sectional area reached a maximum value of 0.19 at a free-stream Mach number of 1.05 and a mass-flow ratio of 0.260.

2. At a Mach number of 1.80, the additive drag coefficient based on the capture area was 0.470 with a mass-flow ratio of 0.612. This value was 20 percent greater than the predicted value for a 25° half-angle single-cone inlet operating under similar off-design conditions.

3. The highest observed value of additive plus cowl pressure drag coefficient for this flight was 0.327 at a free-stream Mach number of 1.81 and a mass-flow ratio of 0.612.

4. The external drag coefficient (cowl pressure plus additive plus friction drag coefficients) increased from 0.140 at a free-stream Mach number of 0.70 to 0.470 at a free-stream Mach number of 1.81. At the low Mach numbers, the friction drag, when compared with the sum of the cowl and additive drags, constituted a large part of the external drag. At the high Mach numbers, the friction drag became a smaller part of the external drag than the cowl plus additive drag. In the transonic Mach number range, the base drag constituted a large part of the total drag. At a free-stream Mach number of 1.07, the base drag amounted to 53 percent of the total drag, while the external drag amounted to 39 percent of the total drag. At a Mach number of 1.80, the external drag amounted to 75 percent of the total, while the base drag amounted to 21 percent of the total.

5. The propulsive thrust coefficient corresponding to the observed rocket-off mass-flow ratios was equal to 0 at a free-stream Mach number of 0.73, a total-temperature ratio of 3.00, and a mass-flow ratio of 0.490; the value increased to 0.540 at a free-stream Mach number of 1.80, a total-temperature ratio of 5.18, and a mass-flow ratio of 0.612. The propulsive thrust coefficient corresponding to an assumed product of fuel-air ratio and combustion efficiency equal to 0.06 was 0.140 at a free-stream Mach number of 0.70, a total-temperature ratio of 7.06, and a mass-flow ratio of 0.319; this value increased to 0.555 at a free-stream Mach number of 1.80, a total-temperature ratio of 5.82, and a mass-flow ratio of 0.567.

6. Comparison between ram-jet engines having approximately the same critical total-temperature ratio but different type inlets and design free-stream Mach numbers (single-cone inlets designed for a free-stream Mach number of 1.8 and double-cone inlets designed for a free-stream Mach number of 2.4) indicated that the transonic propulsive thrust coefficient of the double-cone engine is as much as 69 percent lower than that of the single-cone engine operating at the same total-temperature ratio.

National Advisory Committee for Aeronautics
    Lewis Flight Propulsion Laboratory
        Cleveland, Ohio, August 3, 1954

REFERENCES

1. Kinghorn, George F., and Disher, John H.: Free-Flight Investigation of 16-Inch-Diameter Supersonic Ram-Jet Unit. NACA RM E8A26, 1948.

2. Carlton, William W., and Messing, Wesley E.: Free-Flight Performance of 16-Inch-Diameter Supersonic Ram-Jet Units. I - Four Units Designed for Combustion-Chamber-Inlet Mach Number of 0.12 at Free-Stream Mach Number of 1.6 (Units A-2, A-3, A-4, and A-5). NACA RM E9F22, 1949.

3. Messing, Wesley E., and Simpkinson, Scott H.: Free-Flight Performance of 16-Inch-Diameter Supersonic Ram-Jet Units. II - Five Units Designed for Combustion-Chamber-Inlet Mach Number of 0.16 at Free-Stream Mach Number of 1.60 (Units B-1, B-2, B-3, B-4, and B-5). NACA RM E50B14, 1950.

4. Disher, John H., and Rabinowitz, Leonard: Free-Flight Performance of 16-Inch-Diameter Supersonic Ram-Jet Units. III - Four Units Designed for Combustion-Chamber-Inlet Mach Number of 0.245 at Free-Stream Mach Number of 1.8 (Units D-1, D-2, D-3, and D-4). NACA RM E50D07, 1950.

5. Rabb, Leonard, and North, Warren J.: Free-Flight Performance of 16-Inch-Diameter Supersonic Ram-Jet Units. IV - Performance of Ram-Jet Units Designed for Combustion-Chamber-Inlet Mach Number of 0.21 at Free-Stream Mach Number of 1.6 over a Range of Flight Conditions. NACA RM E50L18, 1951.

6. Messing, Wesley E., and Acker, Loren W.: Transonic Free-Flight Drag Results of Full-Scale Models of 16-Inch-Diameter Ram-Jet Engines. NACA RM E52B19, 1952.

7. Messing, Wesley E., and Rabb, Leonard: Transonic Free-Flight Investigation of the Total Drag and of The Component Drags (Cowl Pressure, Additive, Base, Friction, and Internal) Encountered by a 16-Inch-Diameter Ram-Jet Engine for Mach Numbers from 0.80 to 1.43. NACA RM E52F02, 1952.

8. North, Warren J.: Summary of Free-Flight Performance of a Series of Ram-Jet Engines at Mach Numbers from 0.80 to 2.20. NACA RM E53K17, 1954.

9. Disher, John H., Kohl, Robert C., and Jones, Merle L.: Free-Flight Performance of a Rocket-Boosted, Air-Launched 16-Inch-Diameter Ram-Jet Engine at Mach Numbers up to 2.20. NACA RM E52L02, 1953.

10. Sibulkin, Merwin: Theoretical and Experimental Investigation of Additive Drag. NACA RM E51B13, 1951.
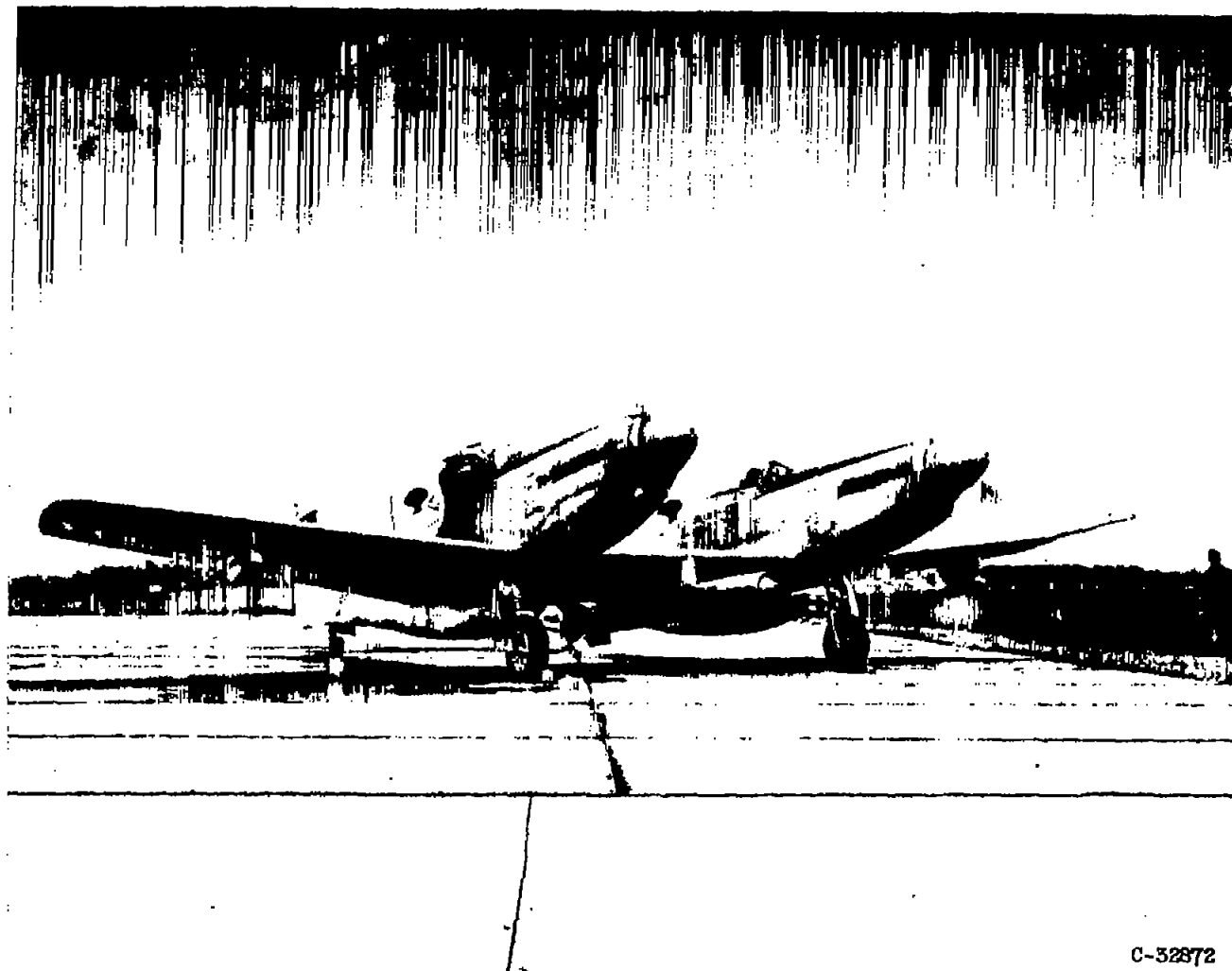
Figure 1. - Photograph of full-scale model mounted beneath center wing panel of F-82 airplane.

C-32872

Gross weight, lb	449
Gross weight minus rocket fuel, lb	347
Inlet flow area, sq ft	0.517
Capture area, sq ft	0.976
Exit flow area, sq ft	0.518
Maximum cross-sectional area, sq ft	1.43

Distance from apex of cone	Centerbody outside radius	Shell inner radius
10.00	4.65	6.84
11.00	5.14	7.12
12.00	5.38	7.20
20.00	5.88	7.67
30.00	6.05	7.92
40.00	5.98	8.00
48.00	5.80	8.00
51.00	5.75	8.00
60.55	5.49	8.00
70.00	5.12	8.00
80.00	4.66	8.00

CD-3493

Figure 2. – Sketch of model including detail of cowl lip. (All dimensions in inches.)
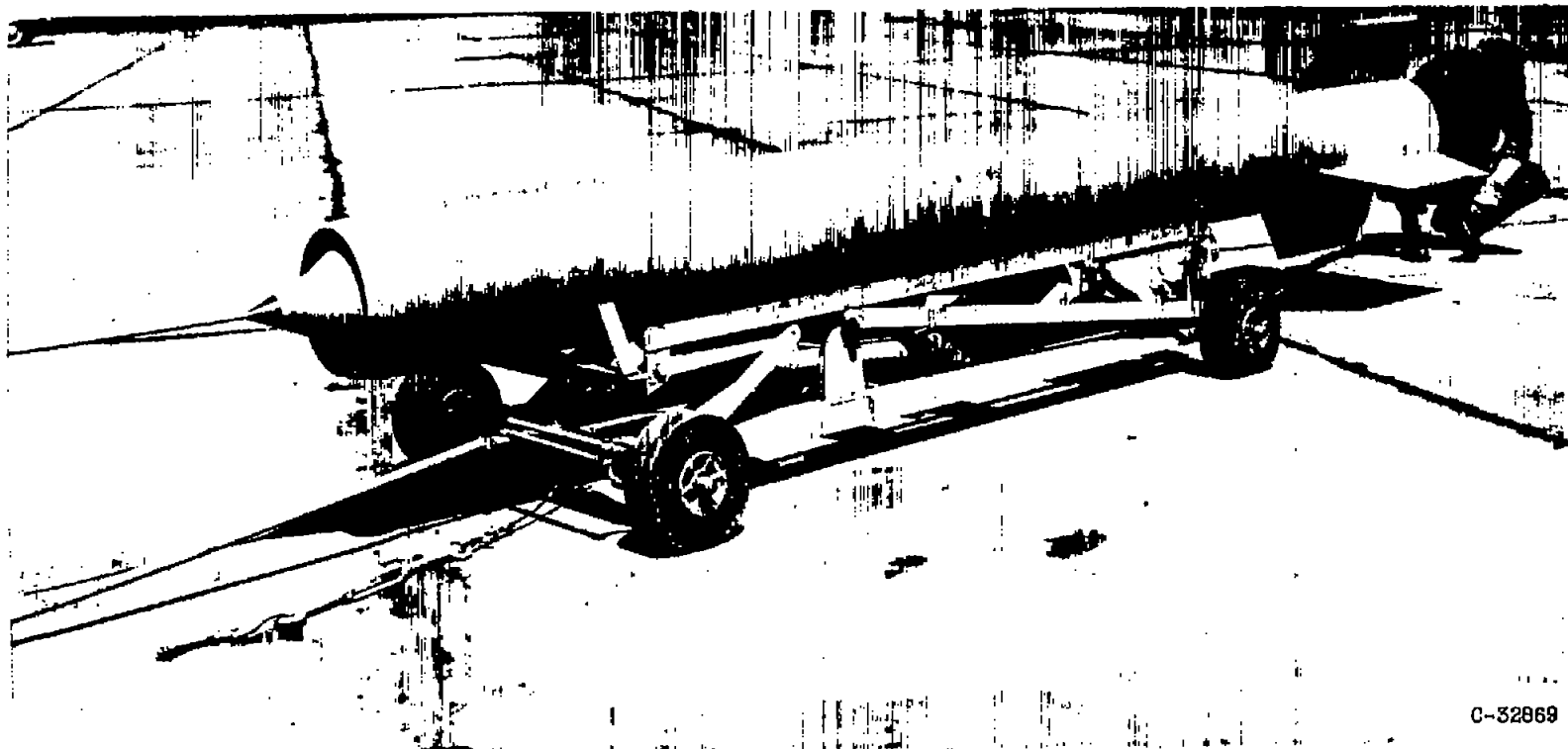
Figure 3. - Full-scale model of 16-inch-diameter ram-jet engine with double-cone inlet.

C-32869
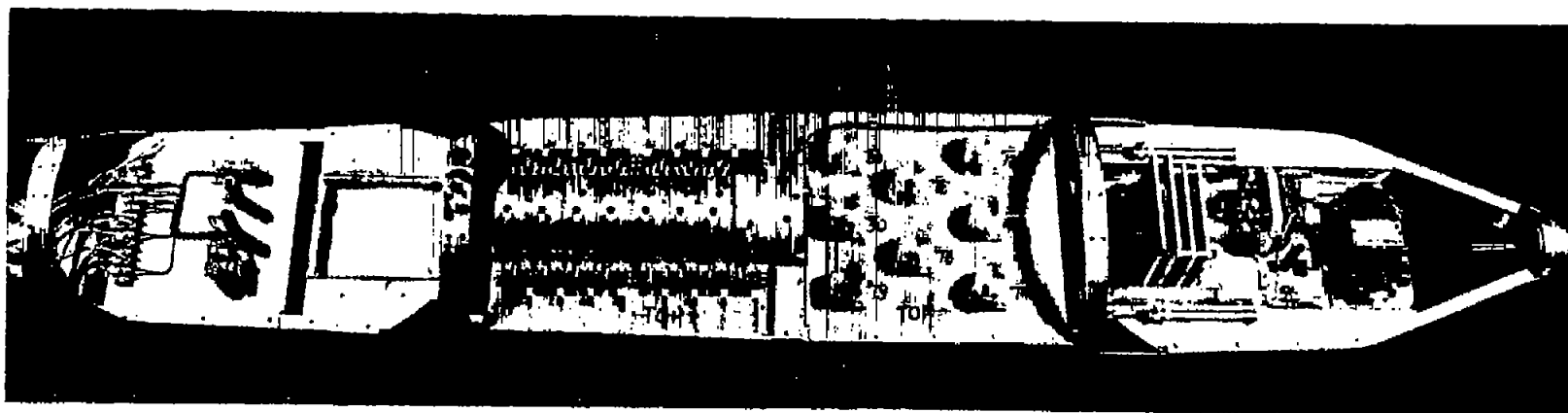
Top view
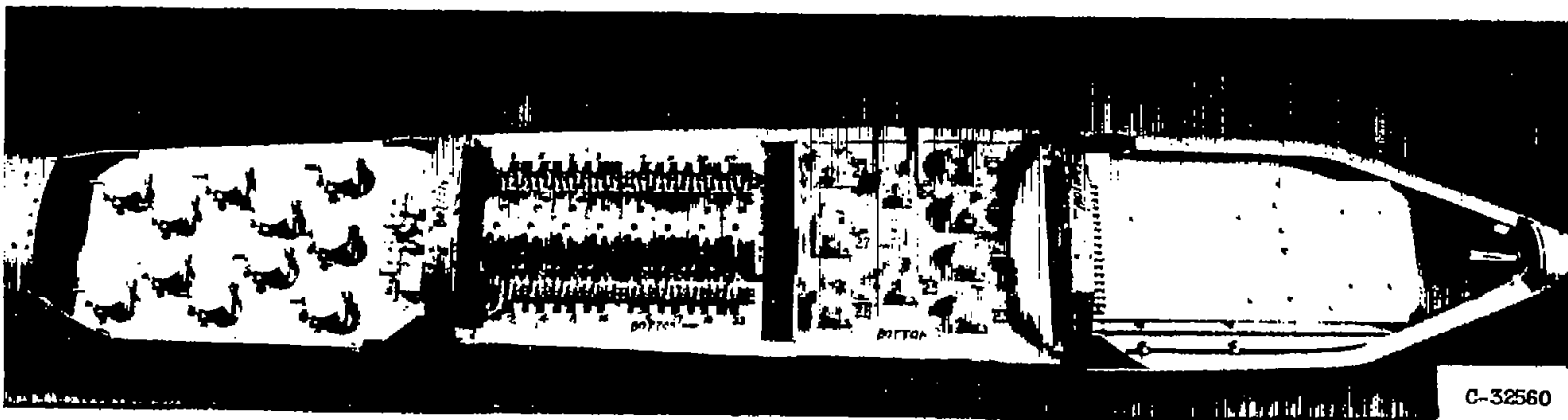
Bottom view

C-32560

Figure 4. - Installation of 10-channel telemetering system with 30 commutable oscillators.
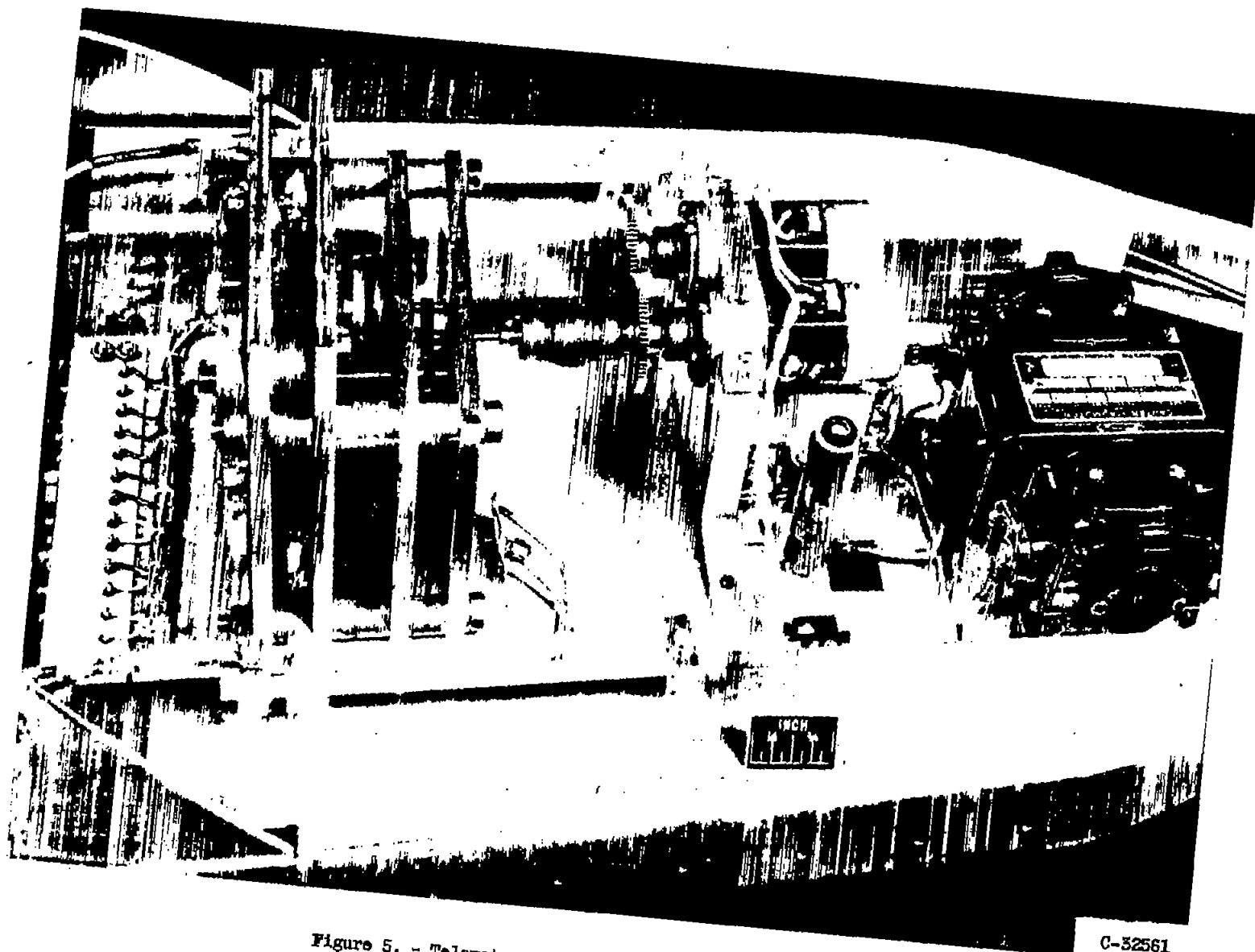
Figure 5. - Telemeter switching-motor assembly installed.

C-32561

C-36412
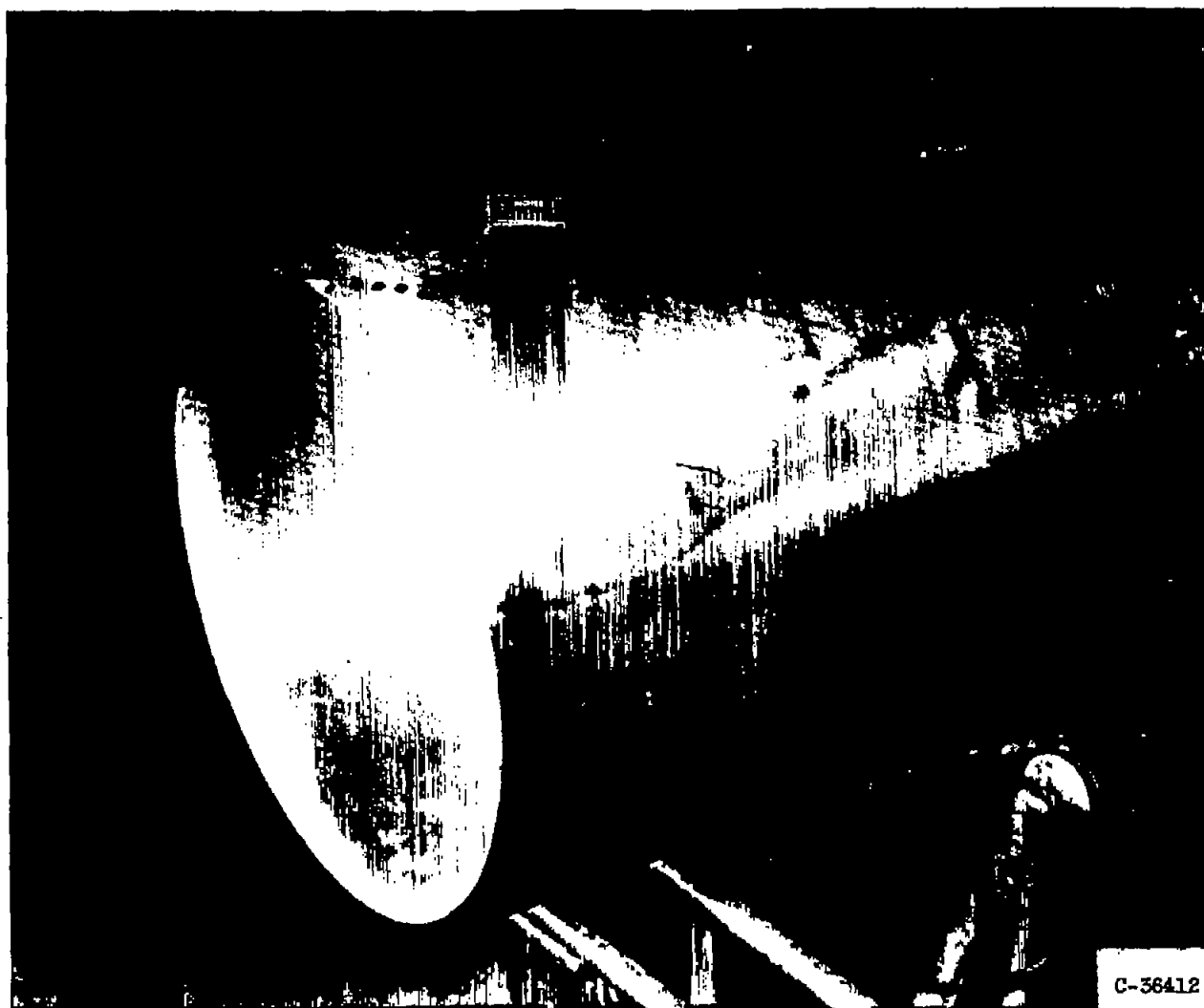
Figure 6. - Outer shell showing location of cowl static-pressure taps.
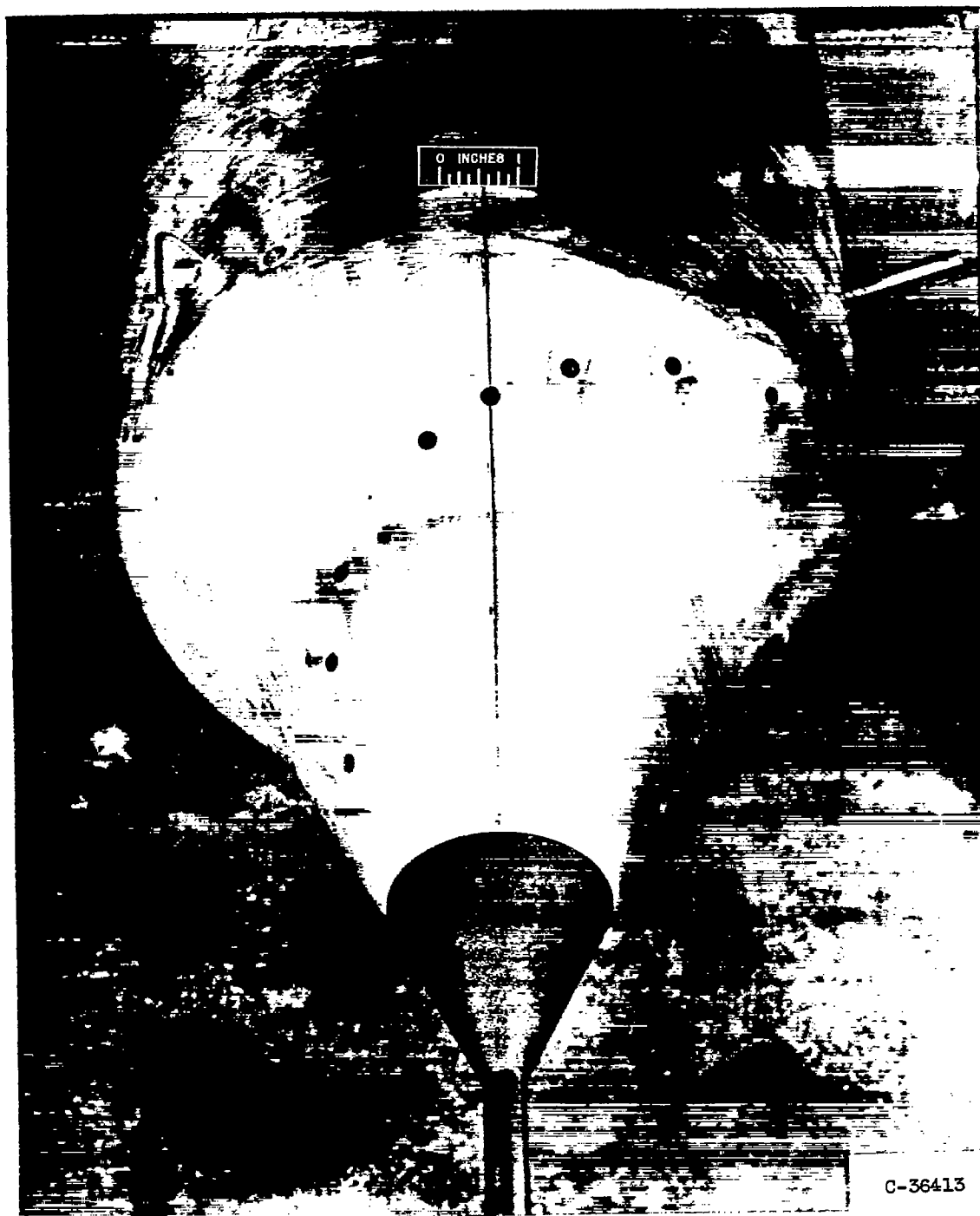
Figure 7. - Forward portion of centerbody showing spike, inlet, and diffuser instrumentation.
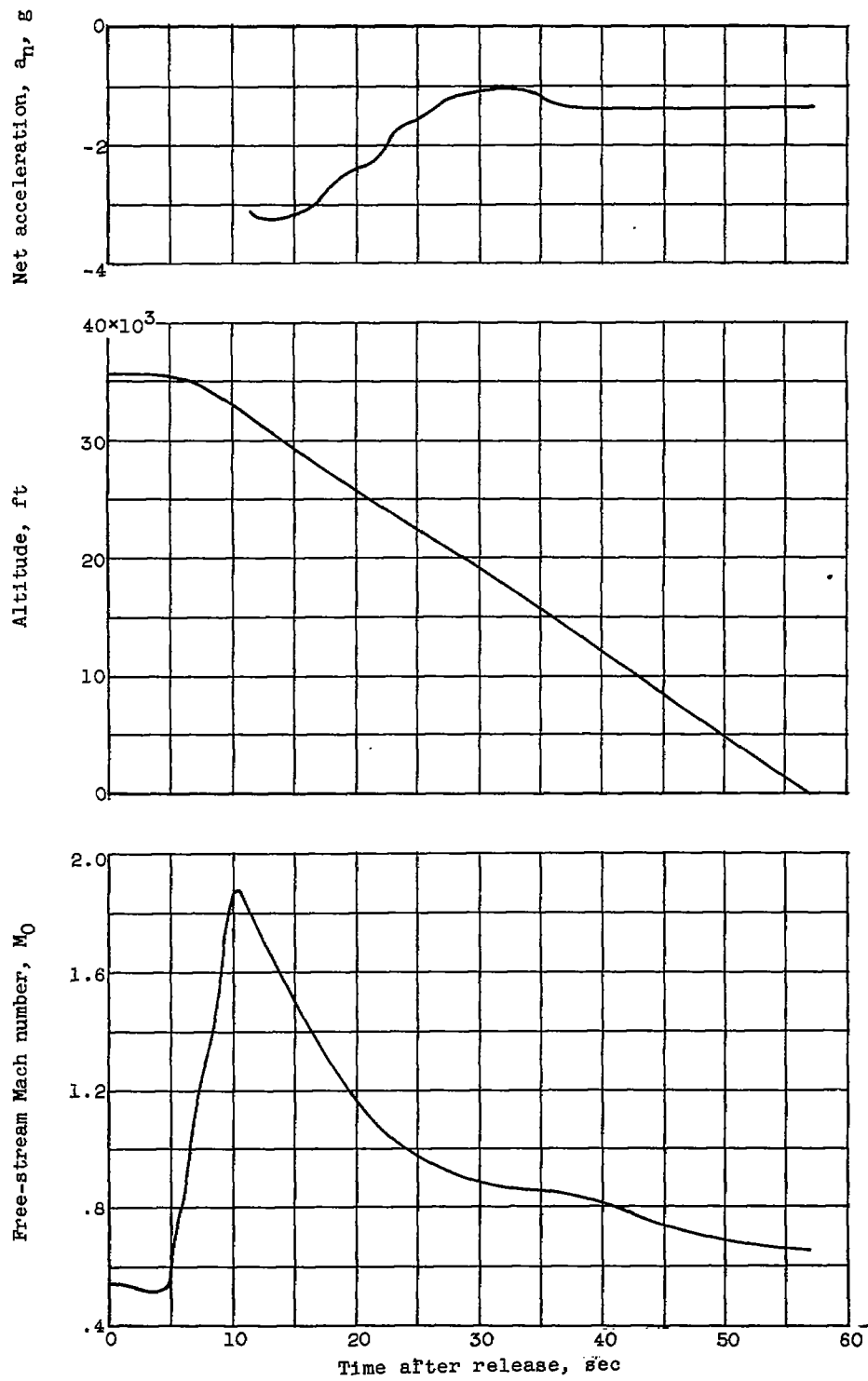
Figure 8. - Time history of flight.

3323

CC-4
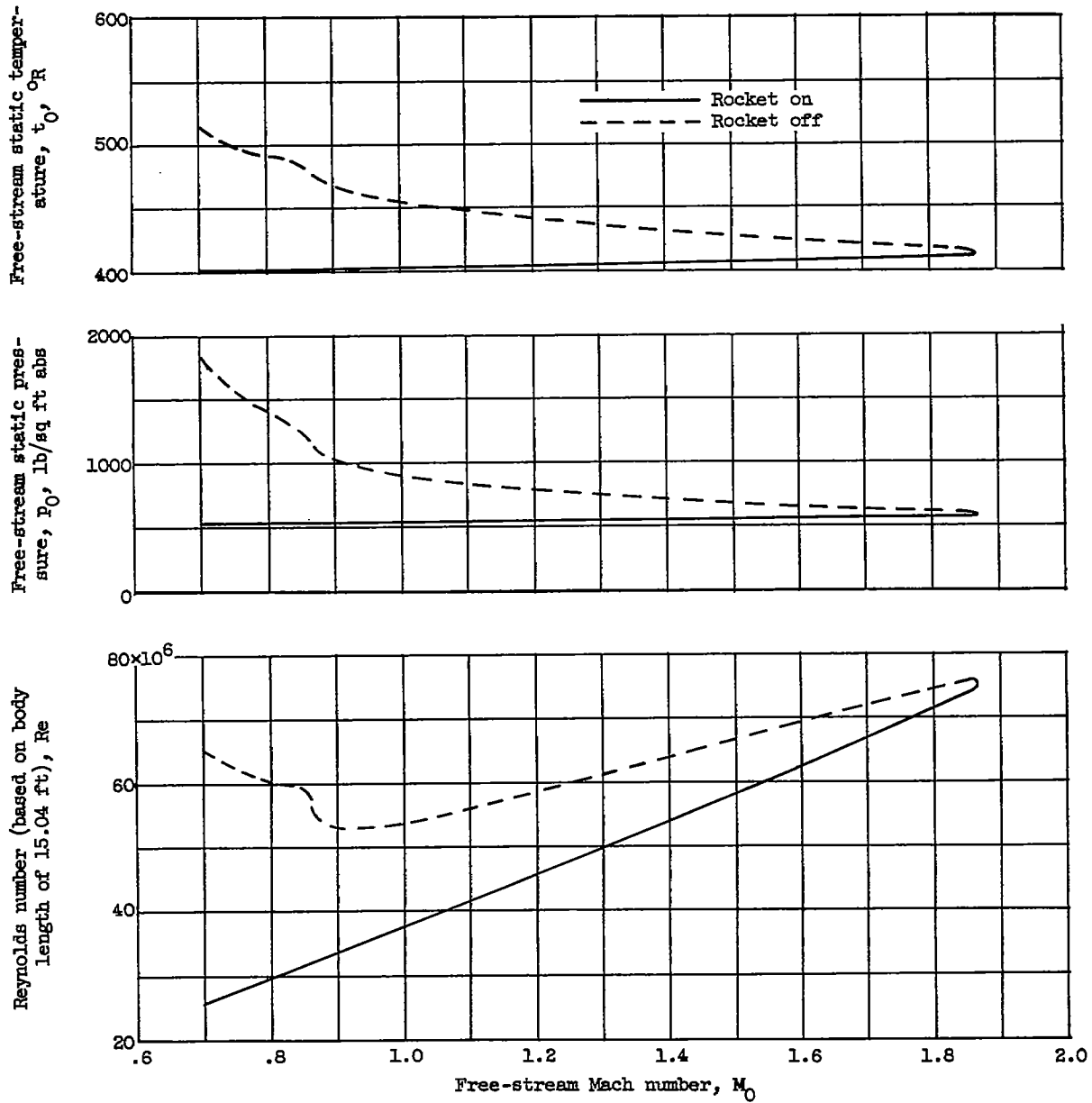
Figure 9. - Free-stream flight conditions against free-stream Mach number.
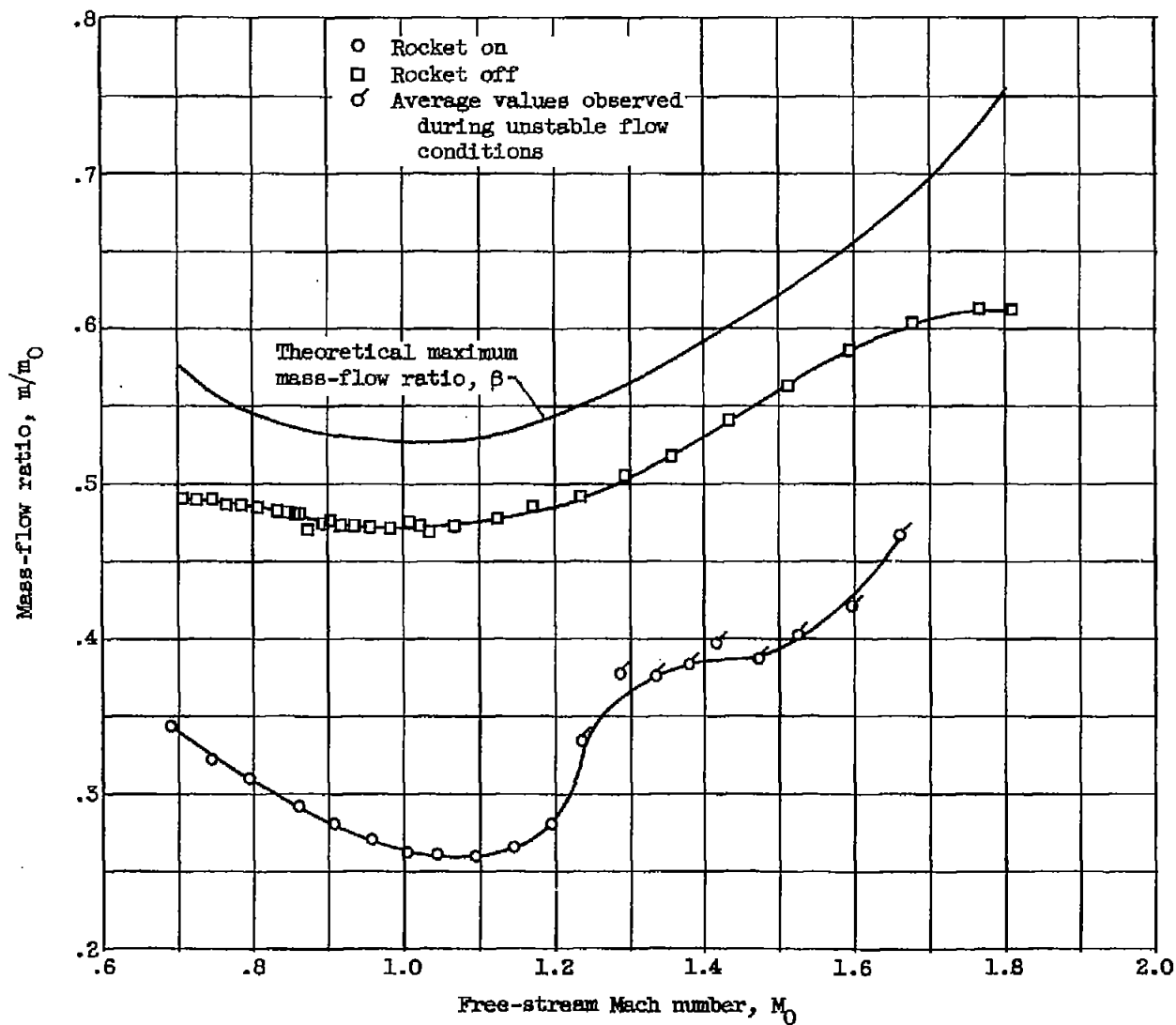
Figure 10. - Variation of mass-flow ratio with free-stream Mach number.
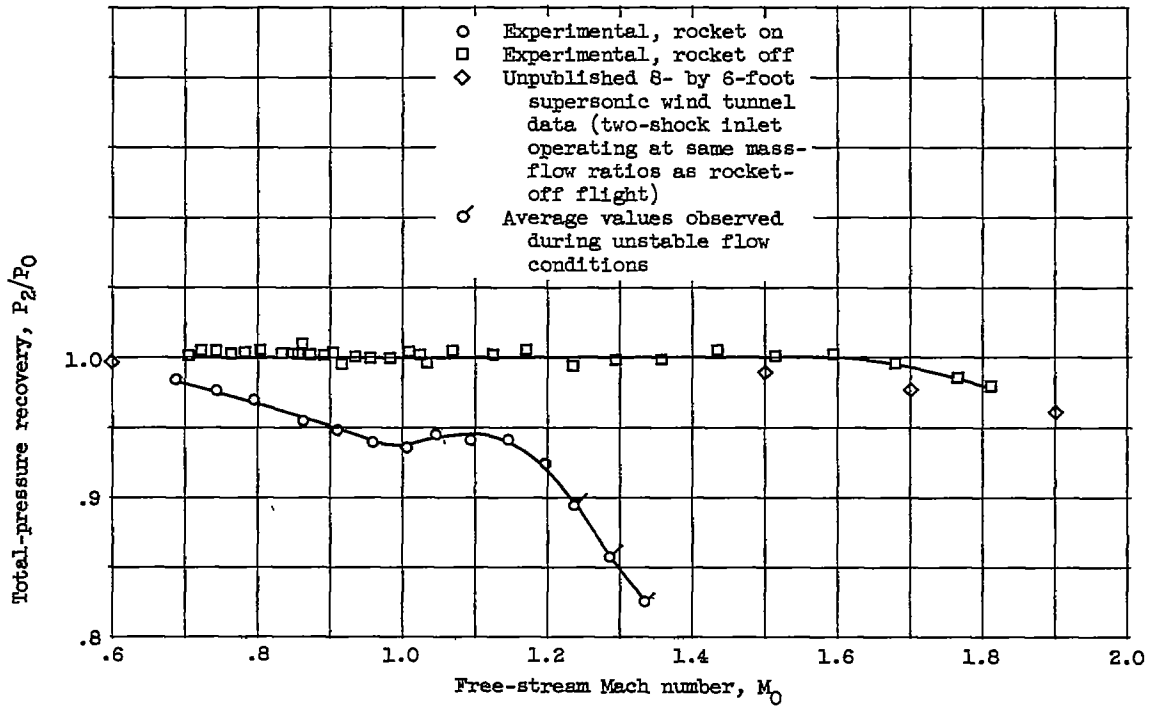
Figure 11. - Effect of free-stream Mach number on total-pressure recovery in diffuser 4.06 inches downstream of inlet.

CONFIDENTIAL

3325

Cowl profile

(a) Free-stream Mach number, 0.70.

$(p_c/p_0)_{sonic}$

Mass-flow ratio, m/m_0

○ 0.541
□ .490

(b) Free-stream Mach number, 0.80.

$(p_c/p_0)_{sonic}$

m/m_0

○ 0.308
□ .485

(c) Free-stream Mach number, 0.90.

$(p_c/p_0)_{sonic}$

m/m_0

○ 0.283
□ .474

Cowl static-pressure ratio, p_c/p_0

Axial distance parameter, S/d
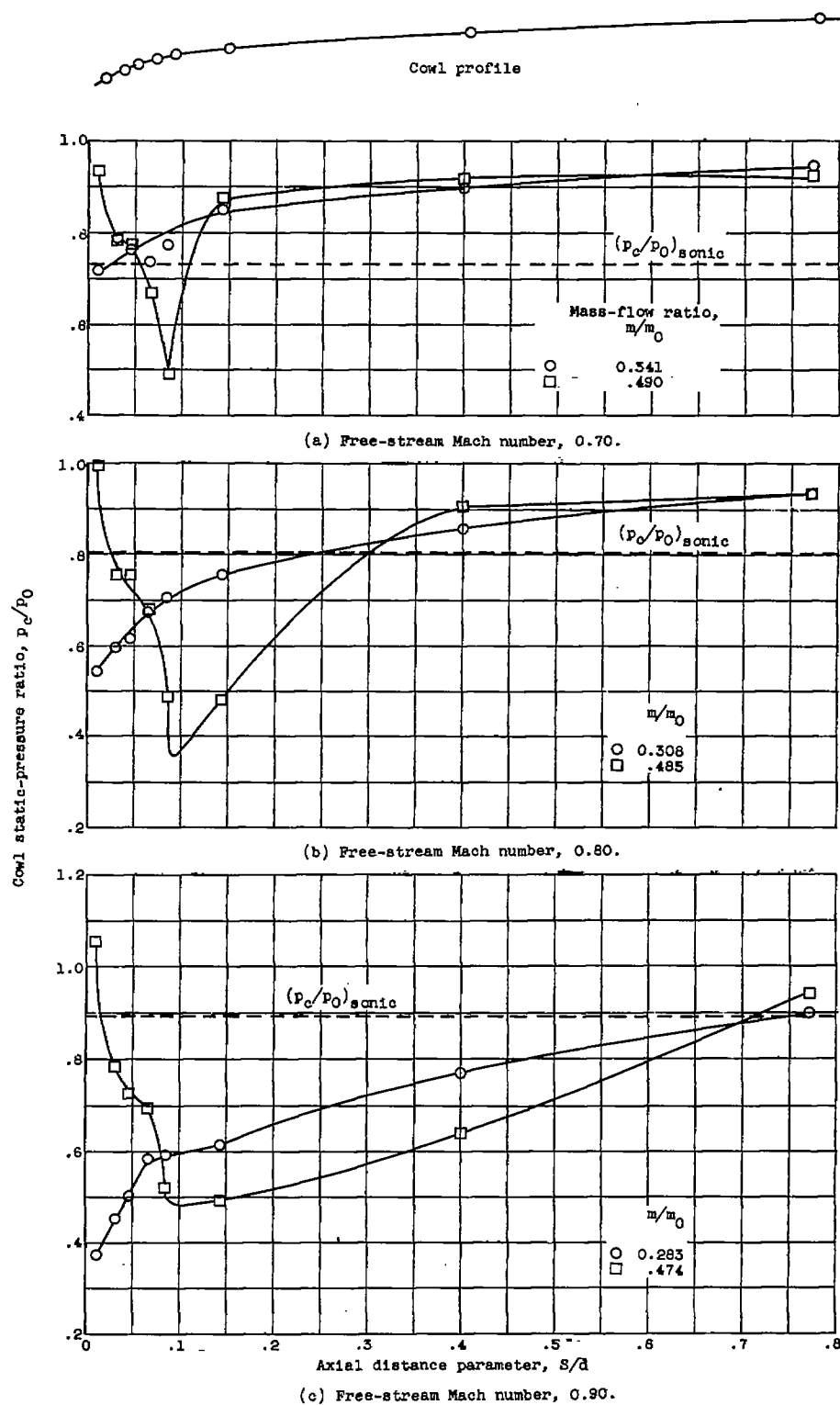
Figure 12. – Effect of mass-flow ratio on cowl-surface pressure distribution.

3323

(d) Free-stream Mach number, 1.00.

(e) Free-stream Mach number, 1.10.

Figure 12. - Continued. Effect of mass-flow ratio on cowl-surface pressure
    distribution.

3323

(f) Free-stream Mach number, 1.20.

Figure 12. - Continued. Effect of mass-flow ratio on cowl-surface pressure
distribution.

3323
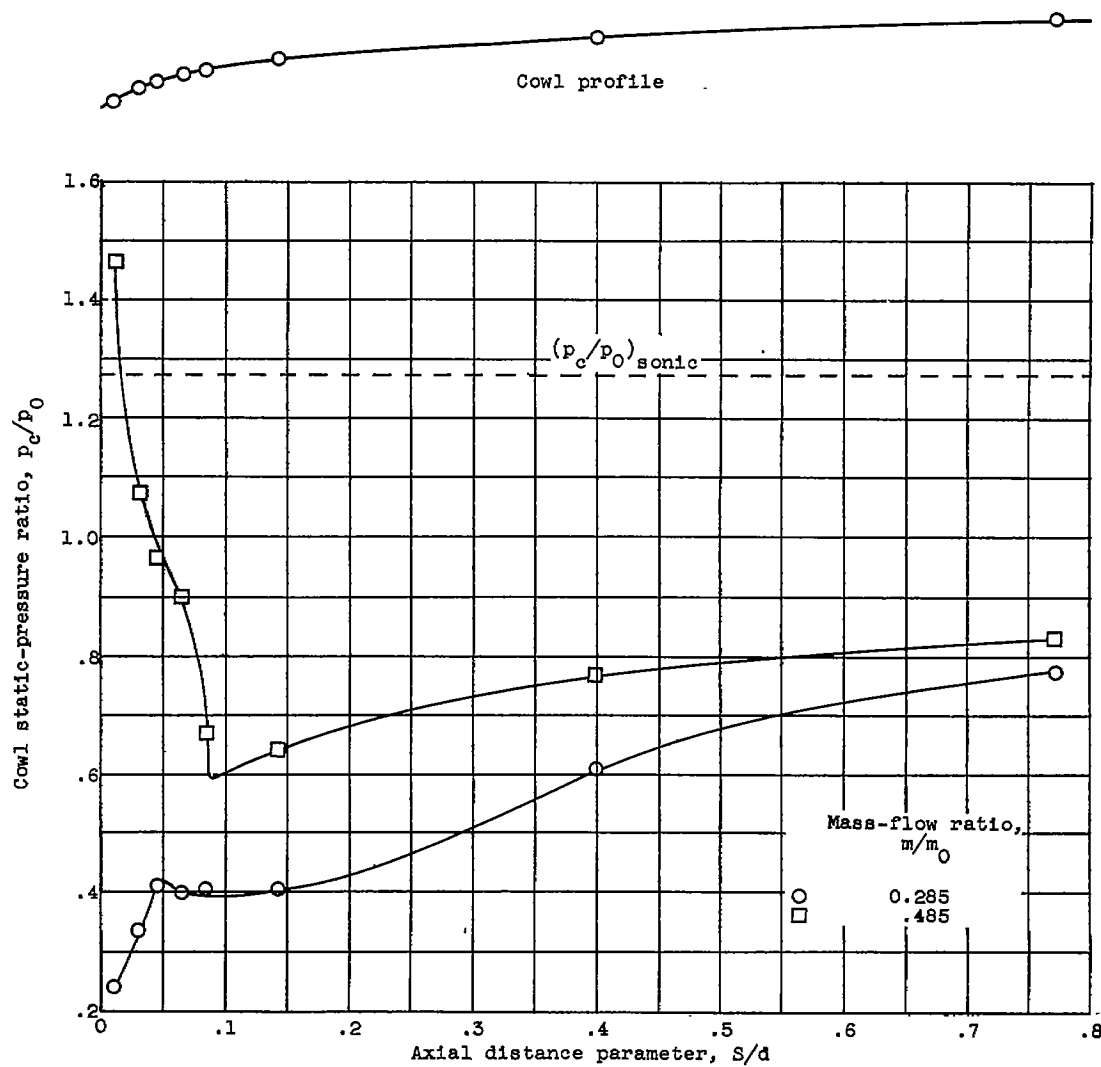
(g) Free-stream Mach number, 1.40.

Figure 12. - Continued. Effect of mass-flow ratio on cowl-surface pressure distribution.
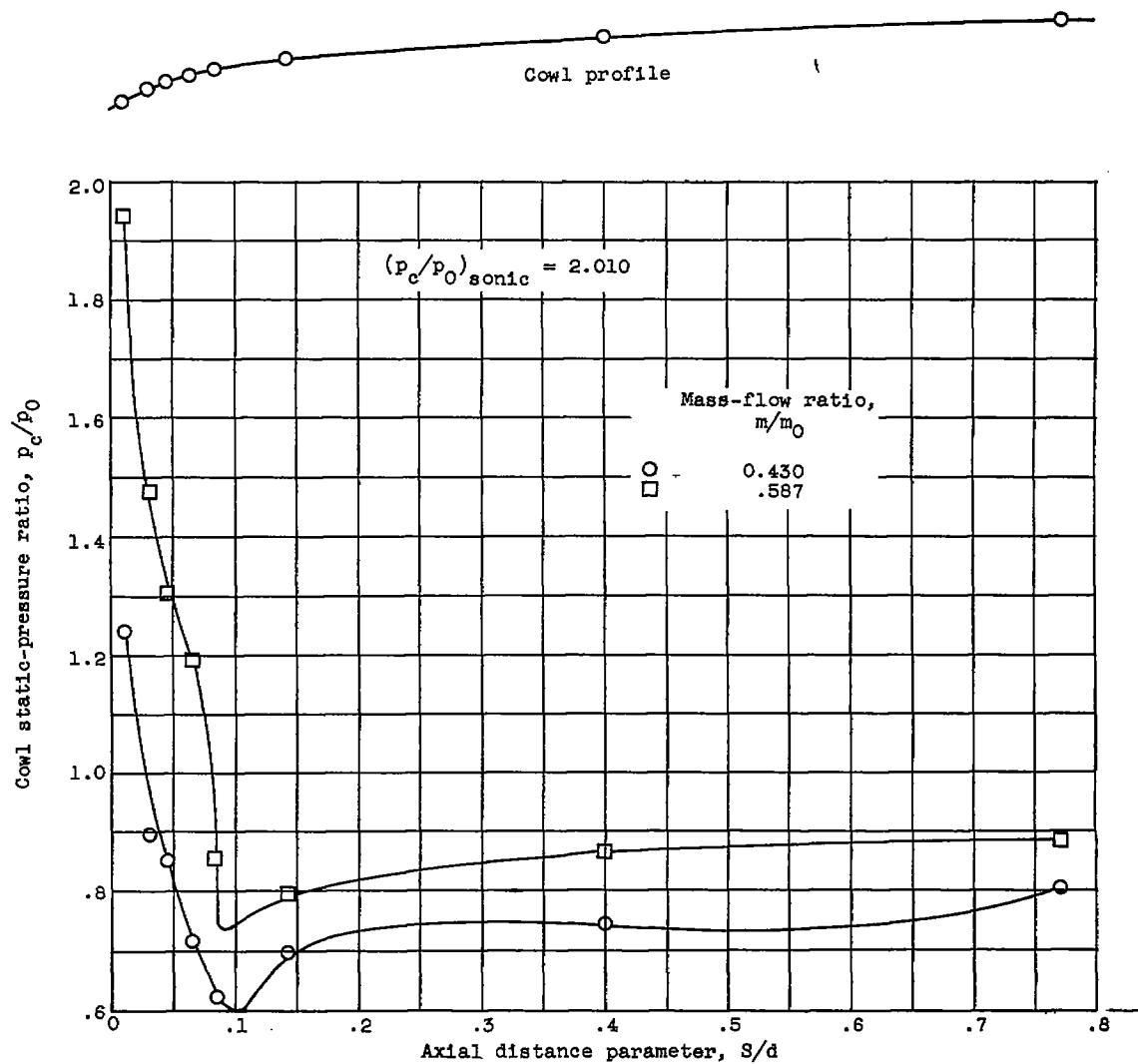
(h) Free-stream Mach number, 1.60.

Figure 12. – Continued. Effect of mass-flow ratio on cowl-surface pressure distribution.
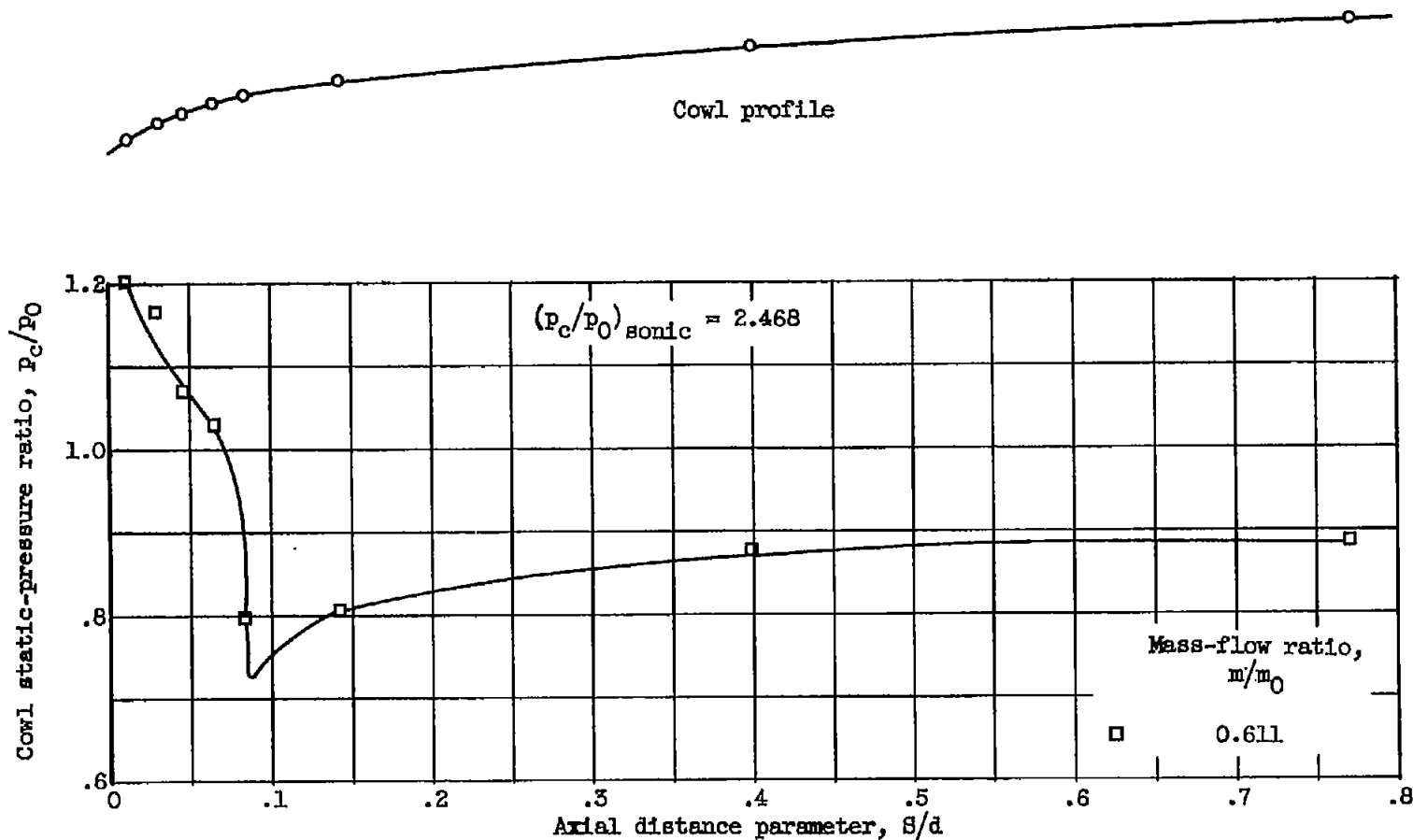
(1) Free-stream Mach number, 1.80.

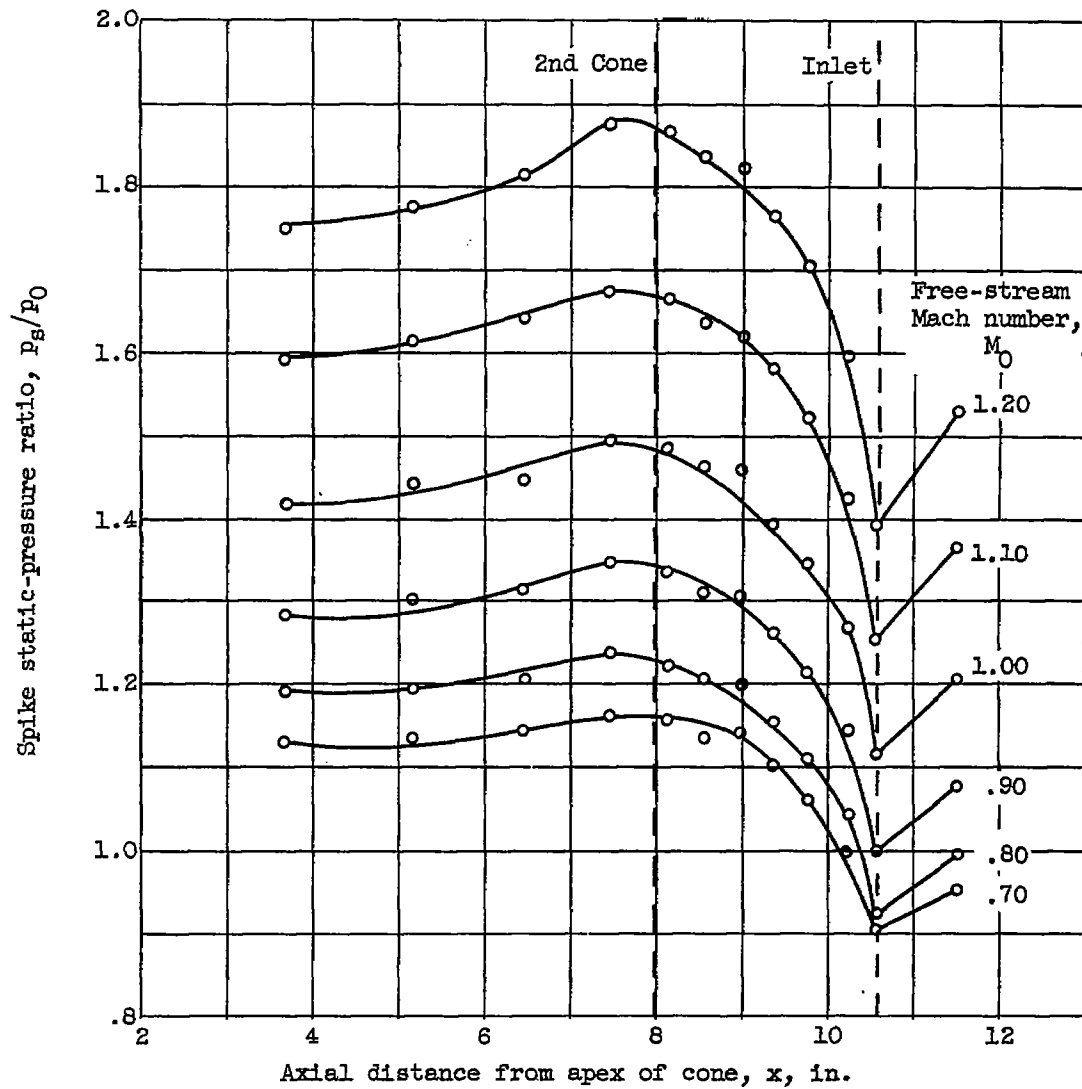Figure 12. - Concluded. Effect of mass-flow ratio on cowl-surface pressure distribution.
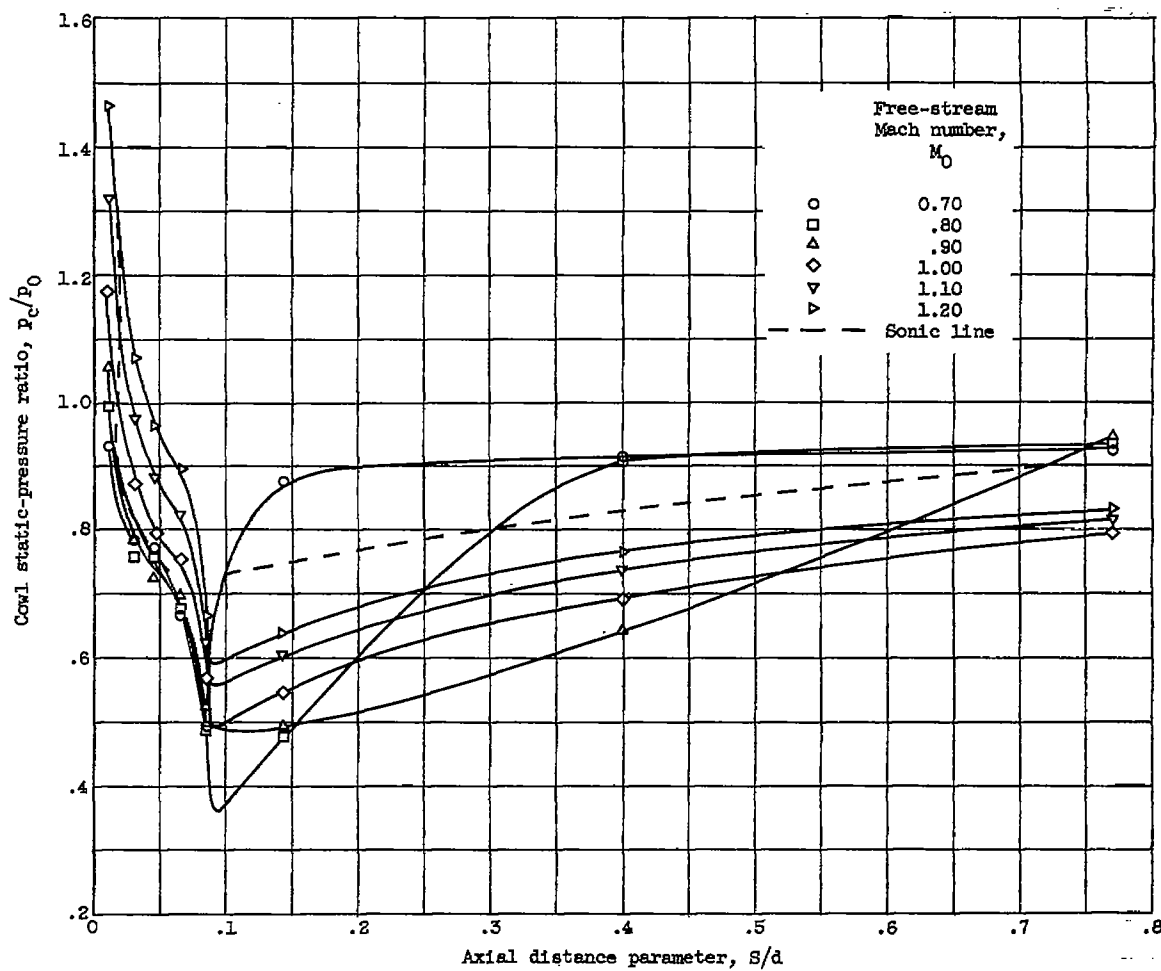
Figure 13. - Effect of free-stream Mach number on cowl-surface pressure distribution at constant mass-flow ratio of approximately 0.48.
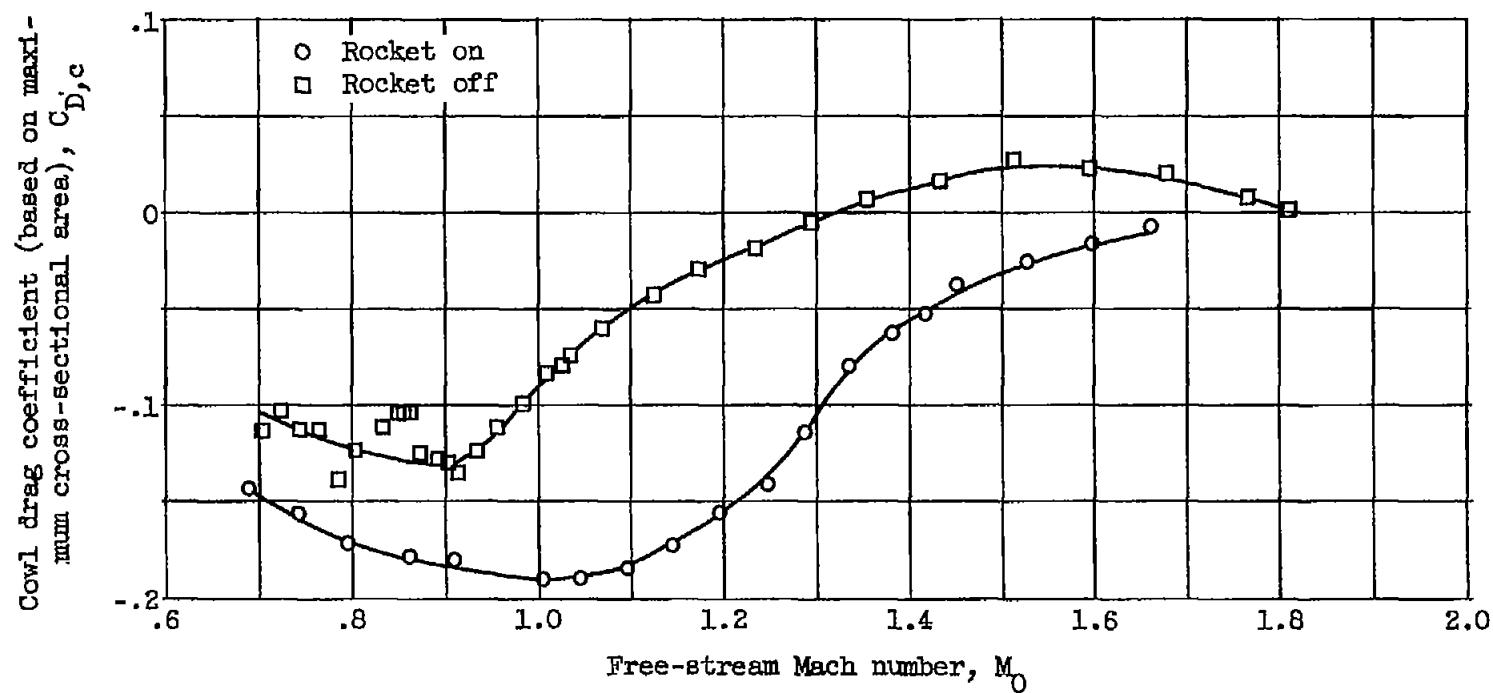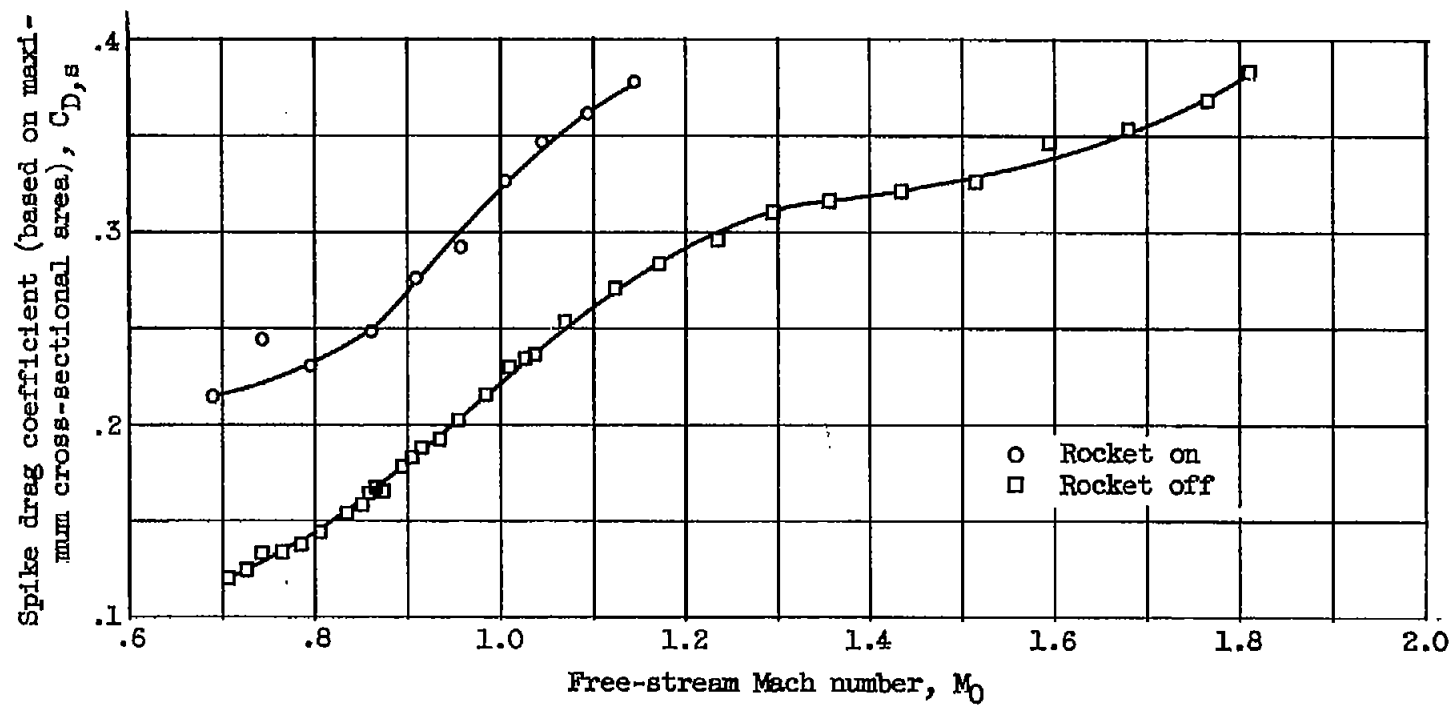
Figure 14. - Effect of free-stream Mach number on cowl pressure drag coefficient.
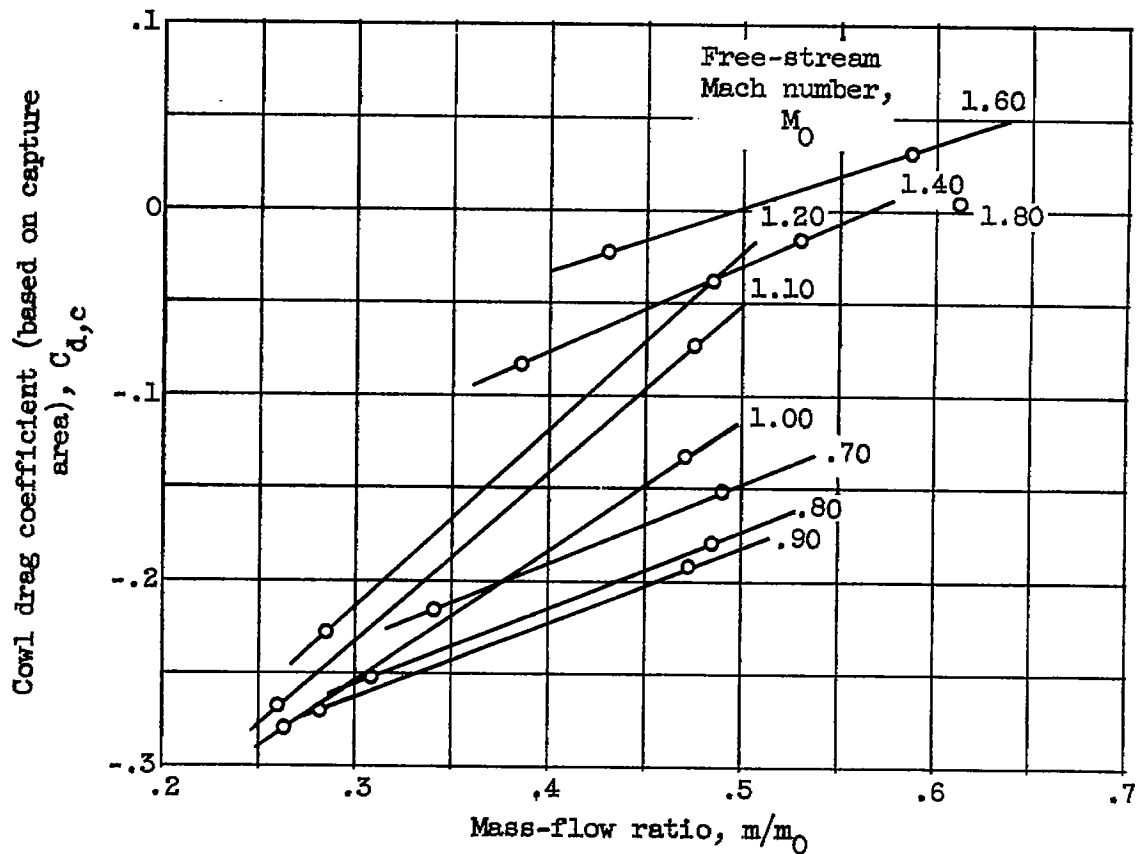
Figure 15. - Effect of mass-flow ratio and free-stream Mach number on cowl pressure drag coefficient.
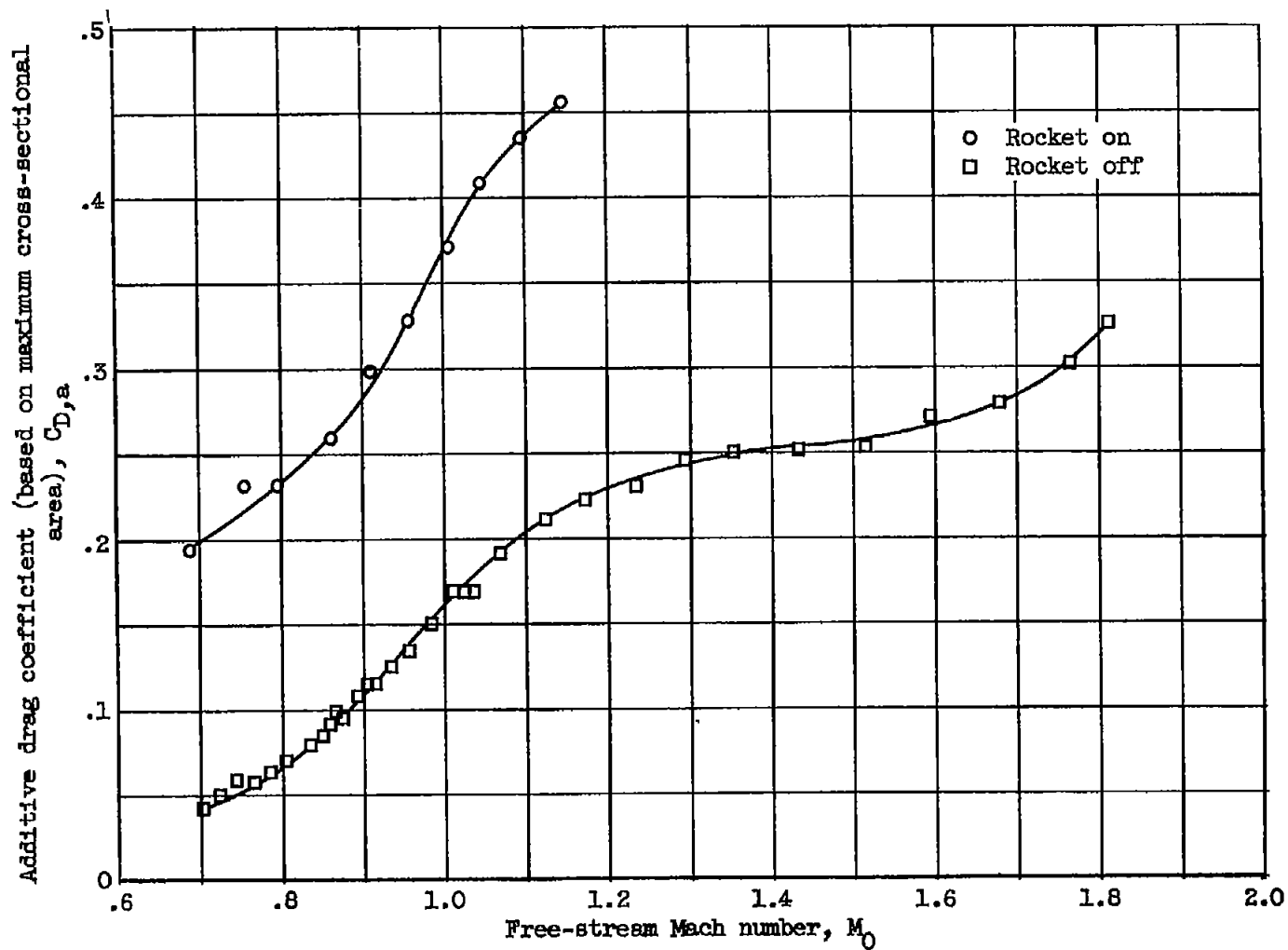
Figure 16. - Effect of free-stream Mach number on additive drag coefficient.
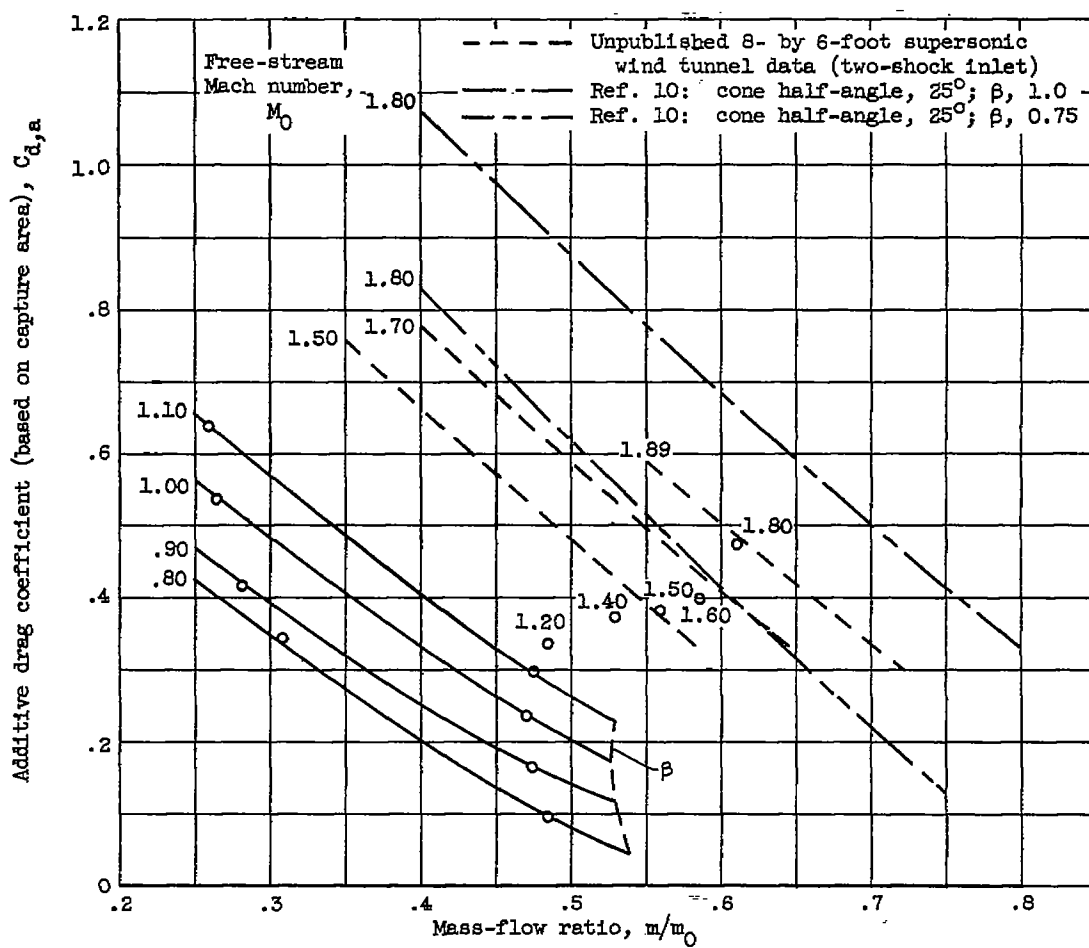
Figure 17. - Effect of mass-flow ratio and free-stream Mach number on additive drag coefficient.
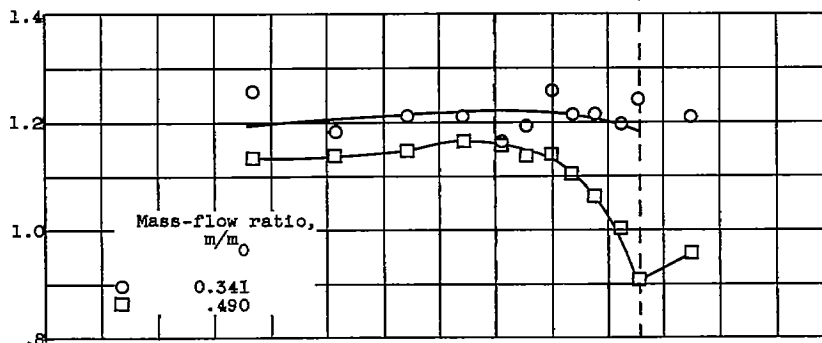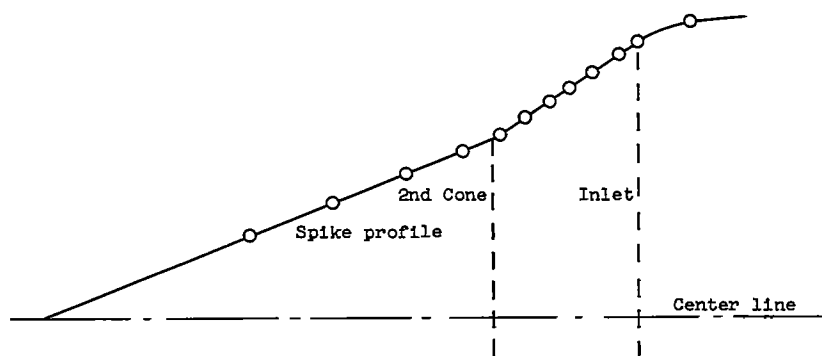
(a) Free-stream Mach number, 0.70.
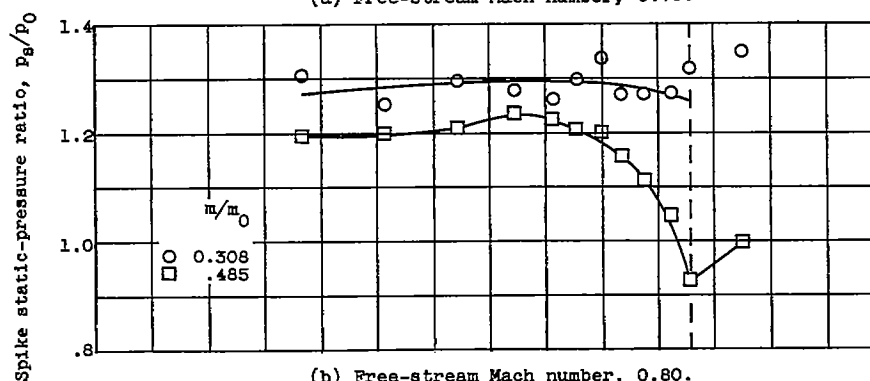
(b) Free-stream Mach number, 0.80.
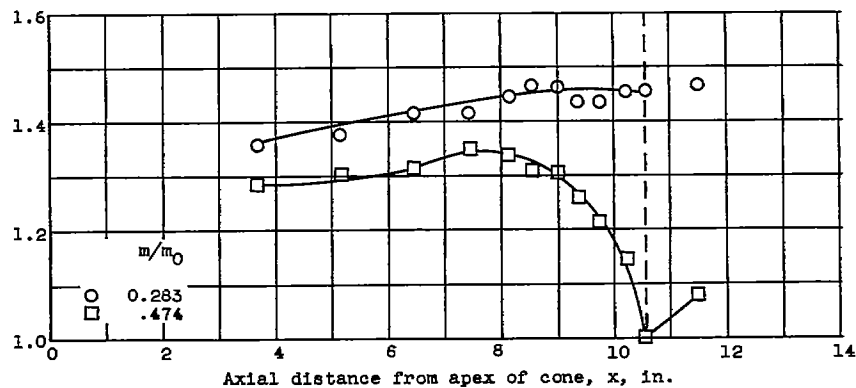
(c) Free-stream Mach number, 0.90.

Figure 18. - Static-pressure distribution along spike.

(d) Free-stream Mach number, 1.00.

(e) Free-stream Mach number, 1.10.

Figure 18. - Continued. Static-pressure distribution along spike.

(f) Free-stream Mach number, 1.20.

(g) Free-stream Mach number, 1.40.

Figure 18. - Continued. Static-pressure distribution along spike.

(h) Free-stream Mach number, 1.60.

Figure 18. - Continued. Static-pressure distribution along spike.

(1) Free-stream Mach number, 1.80.
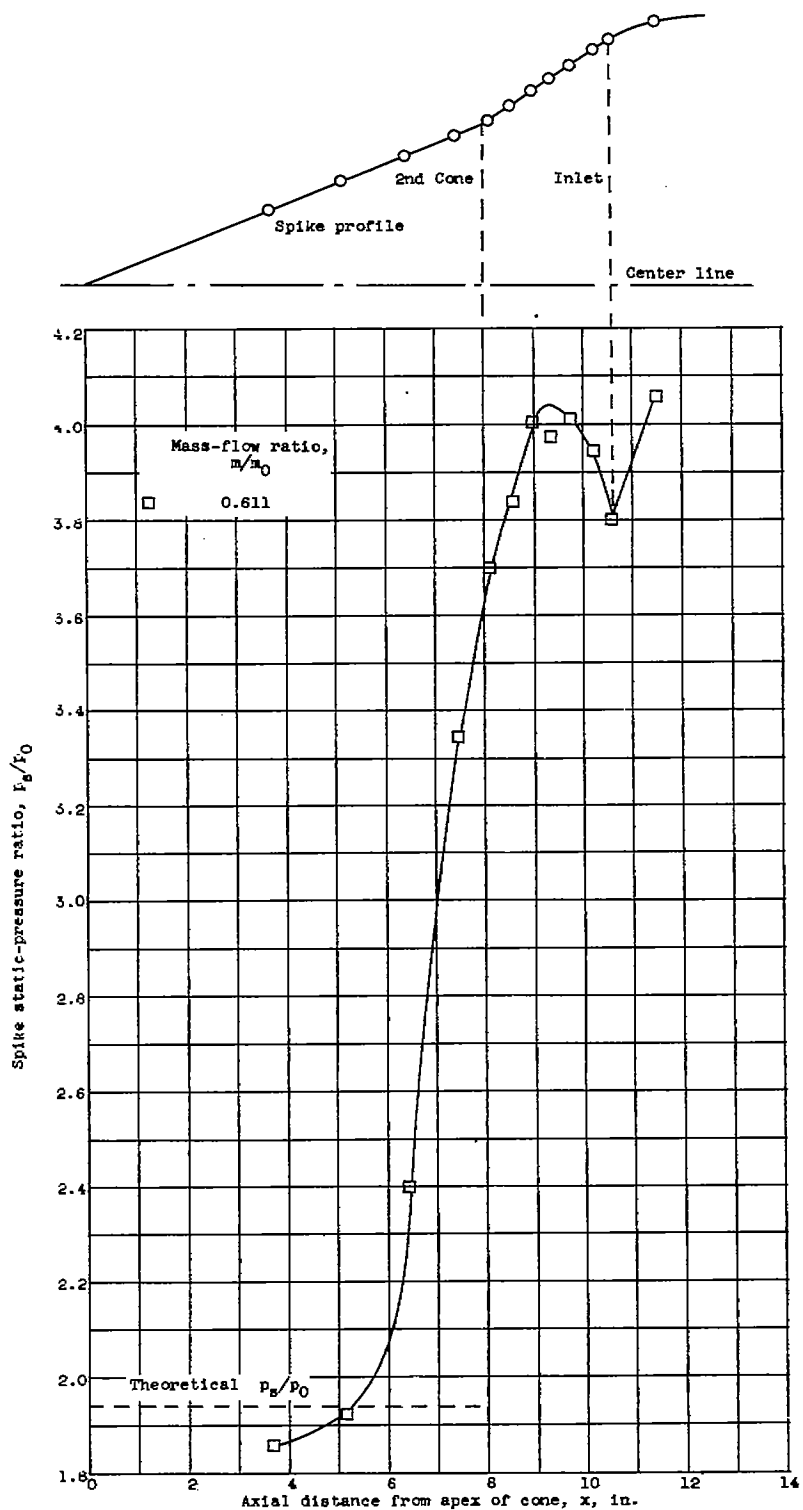
Figure 18. – Concluded. Static-pressure distribution along spike.

Figure 19. - Effect of free-stream Mach number on spike-surface pressure distribution at constant mass-flow ratio of approximately 0.48.

Figure 20. - Effect of free-stream Mach number on spike drag coefficient.

Figure 21. - Effect of free-stream Mach number and mass-flow ratio on additive plus cowl drag coefficients.
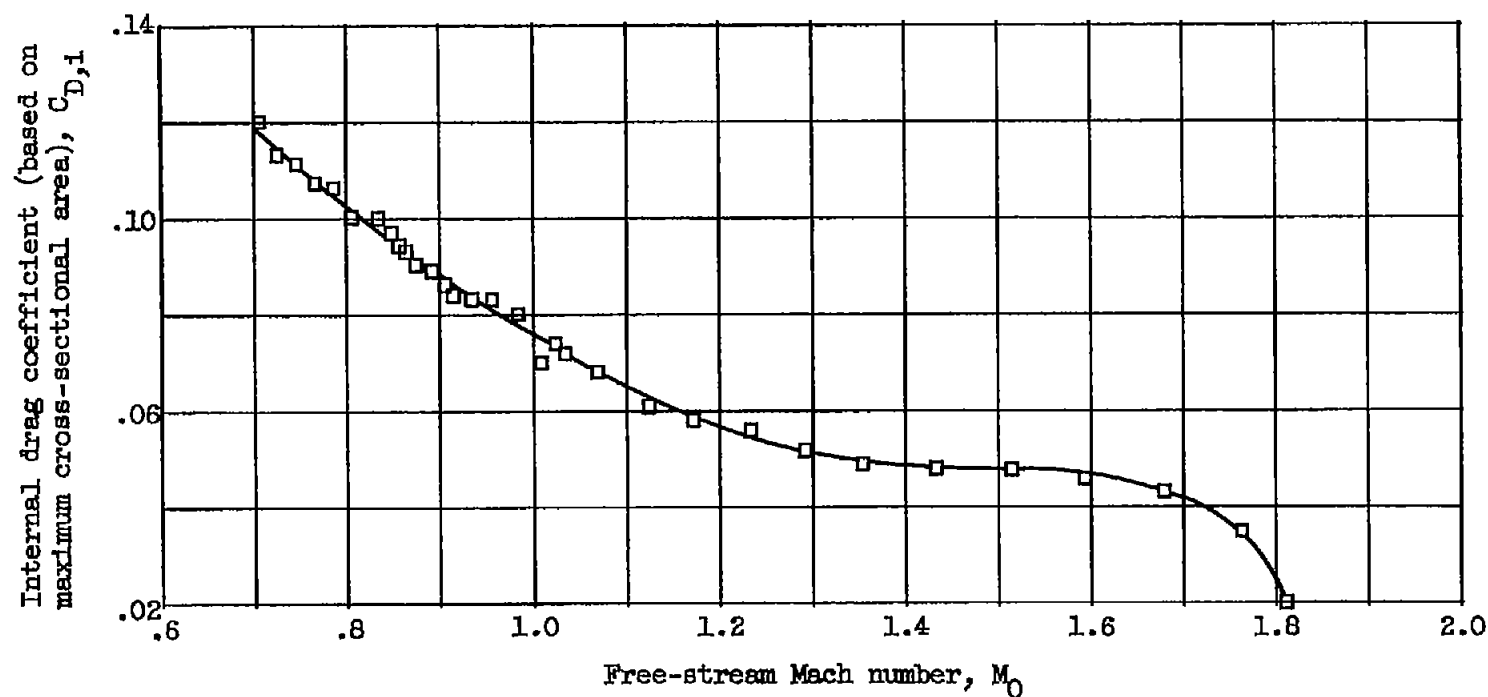
Figure 22. - Effect of free-stream Mach number on internal drag coefficient for rocket-off conditions.
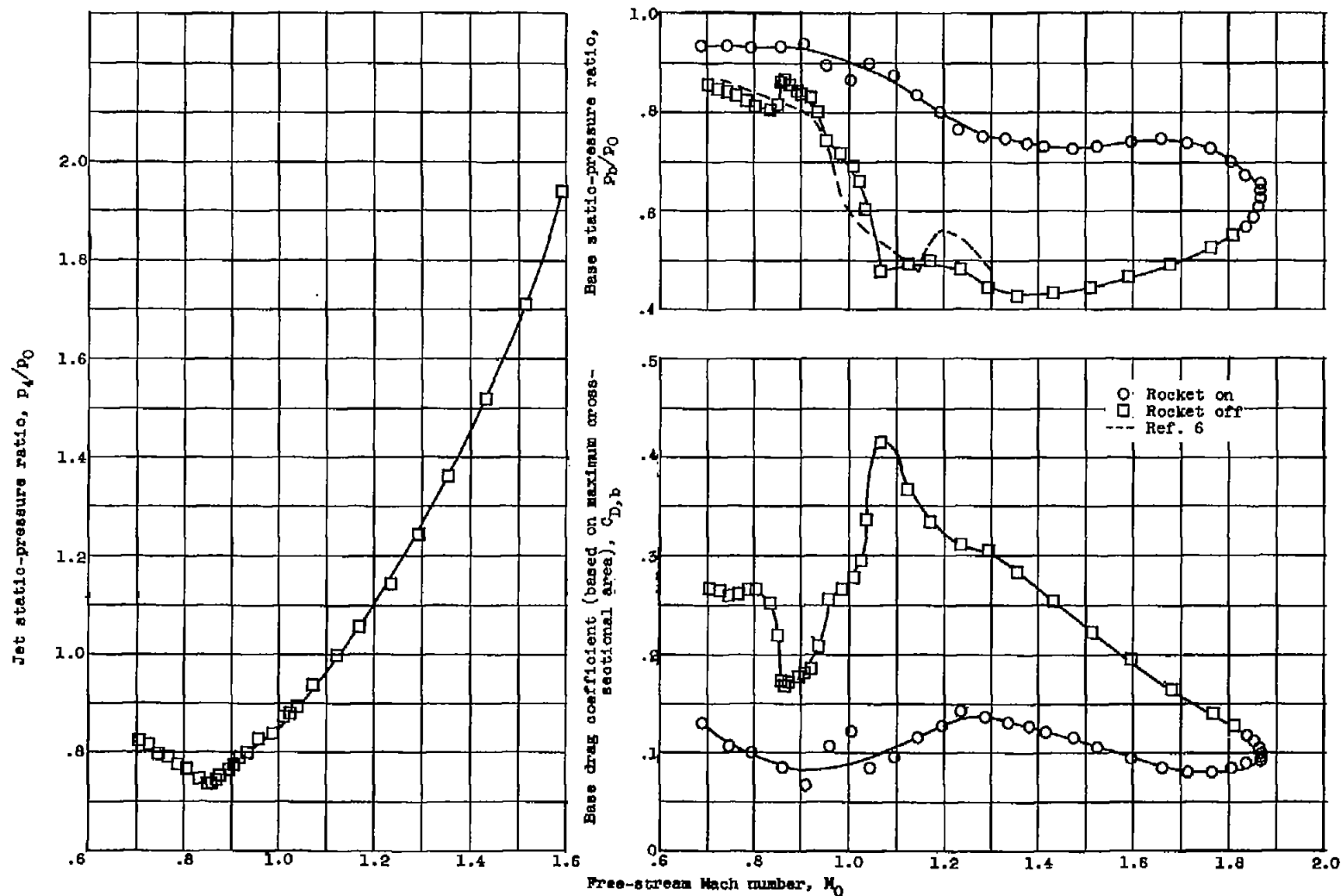
Figure 23. - Effect of free-stream Mach number on jet and base static-pressure ratios and base drag coefficient.

CC-7
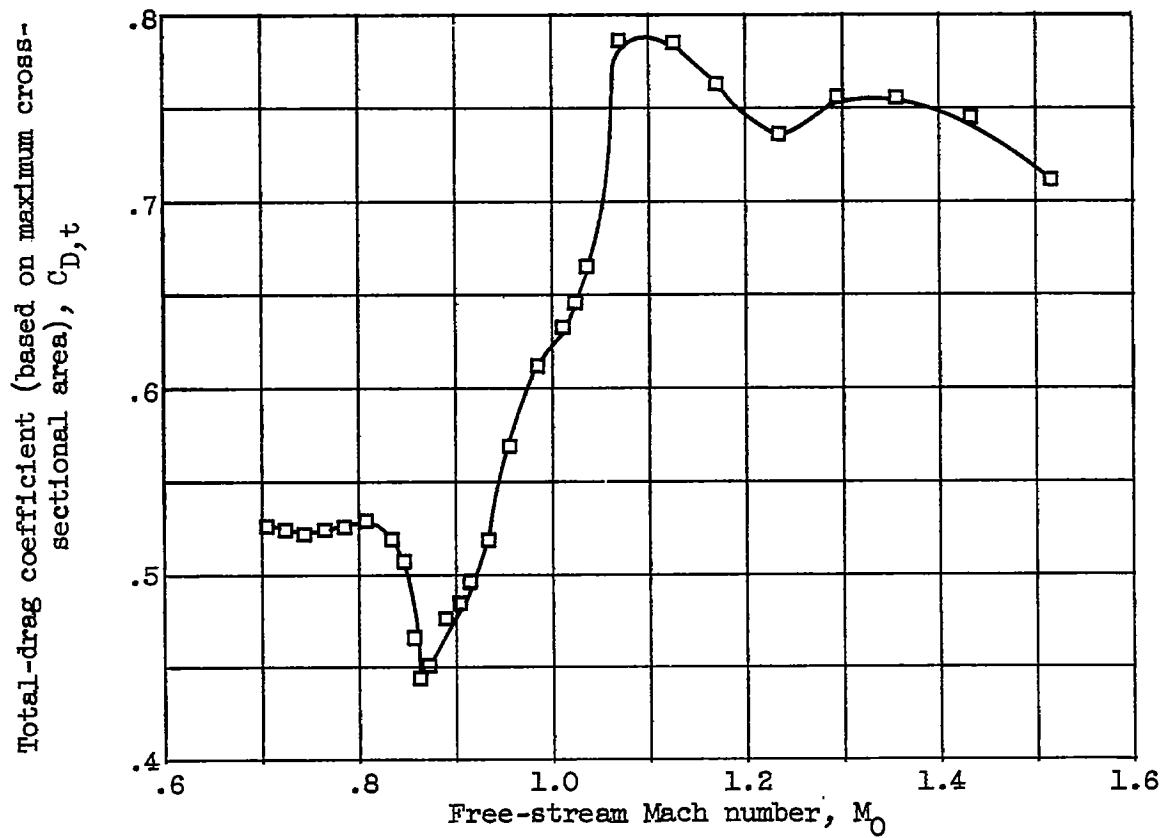
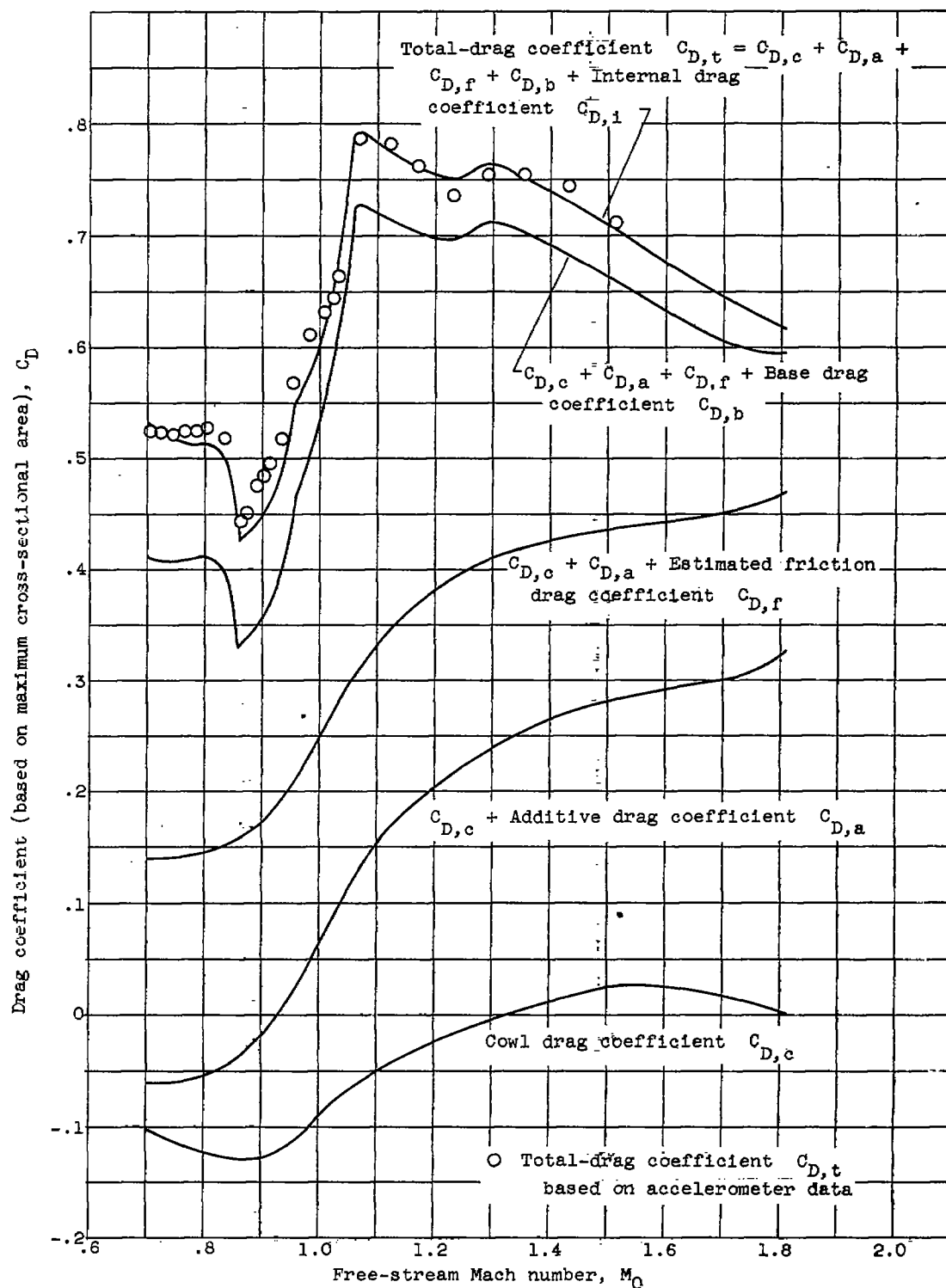Figure 24. - Effect of free-stream Mach number on total-drag coefficient for rocket-off conditions.

Figure 25. - Component and total-drag coefficients against free-stream Mach number for rocket-off conditions.
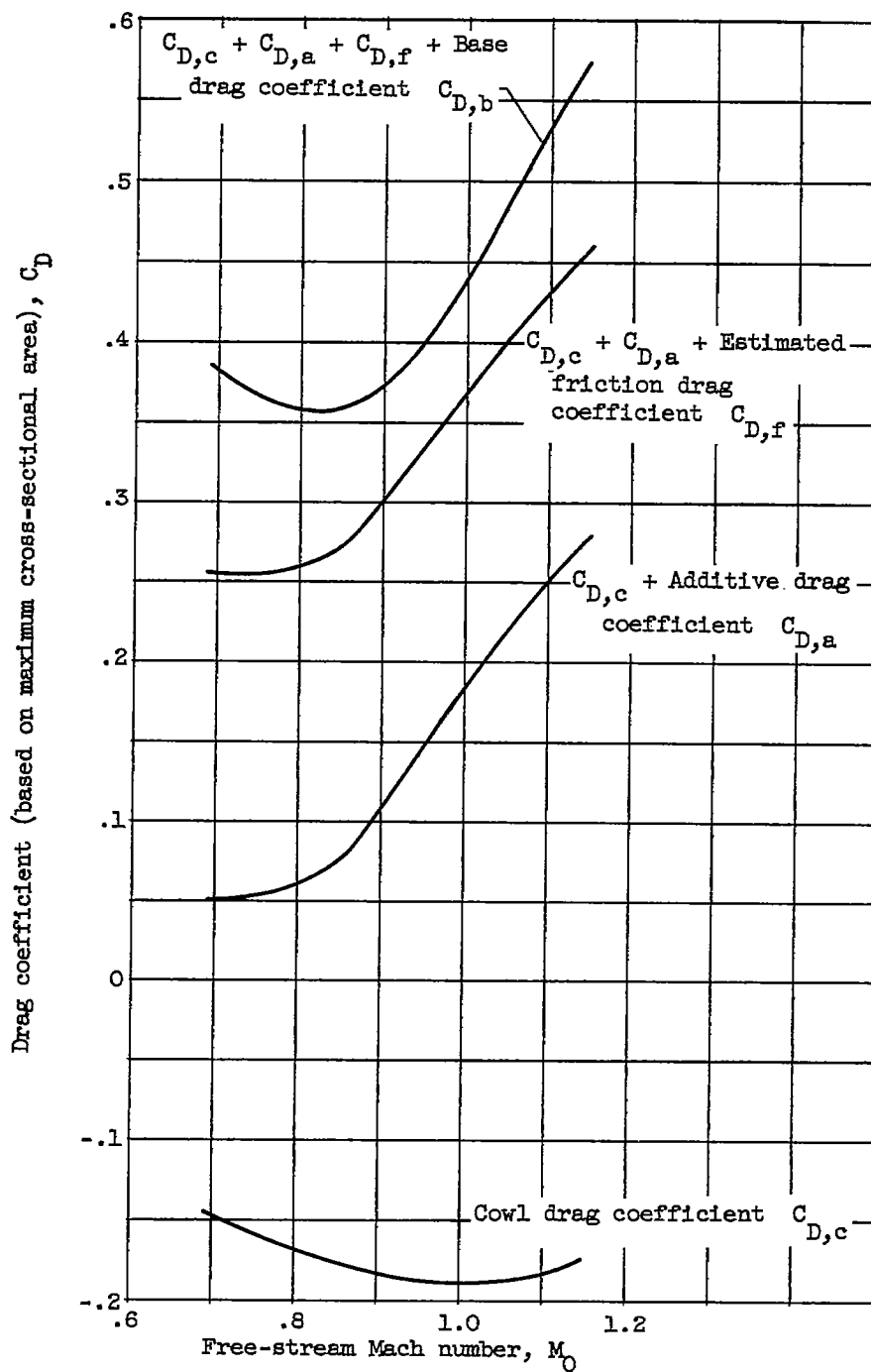
Figure 26. - Component drag coefficients against
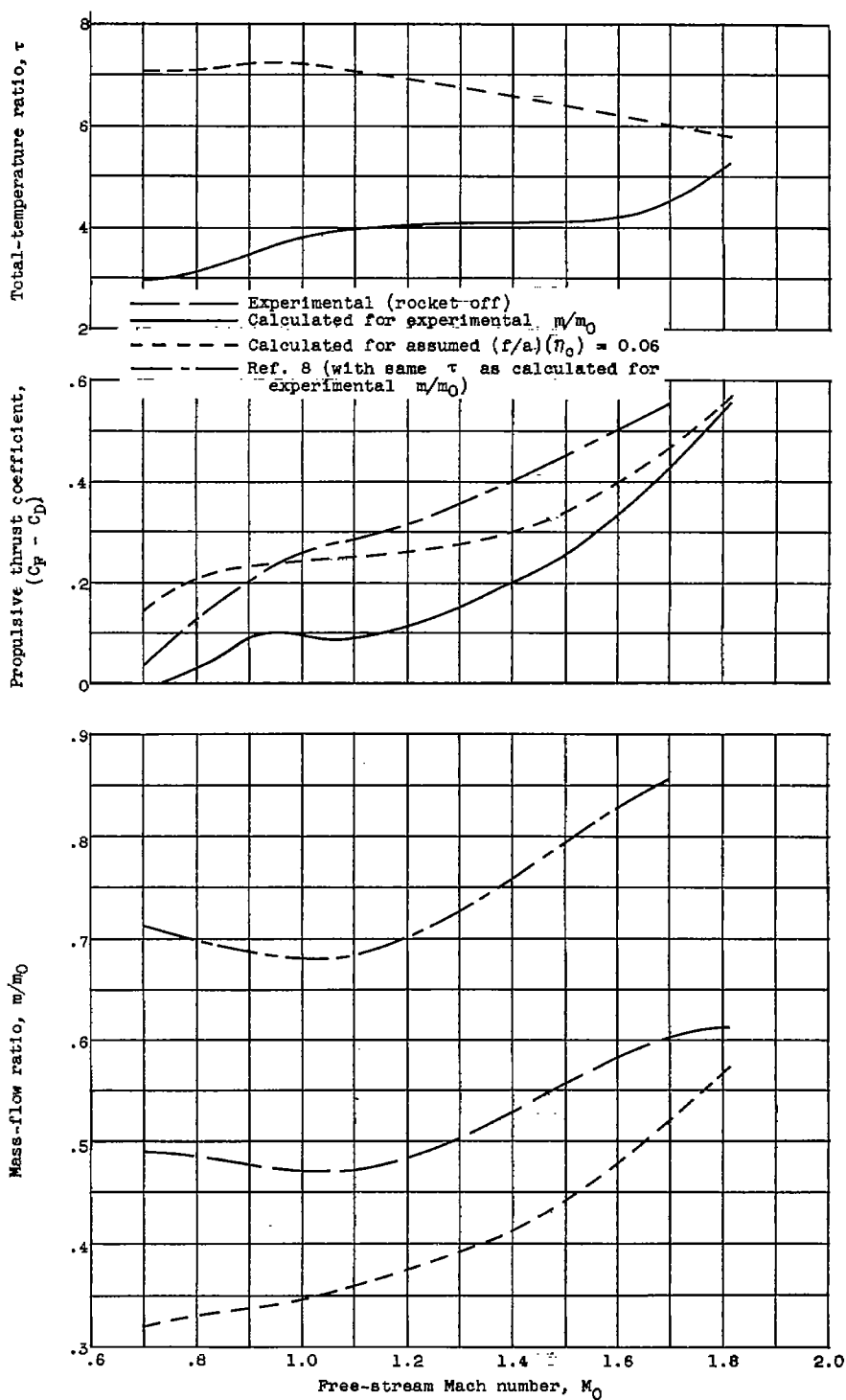free-stream Mach number for rocket-on conditions.

Figure 27. - Simulated total-temperature ratios, propulsive thrust coefficients, and corresponding mass-flow ratios as a function of free-stream Mach number.